HIGH-SPEED AUTOMATIC SCANNING SYSTEM FOR EMULSION ANALYSIS IN THE OPERA EXPERIMENT

A THESIS SUBMITTED TO
THE GRADUATE SCHOOL OF NATURAL AND APPLIED SCIENCES
OF
MIDDLE EAST TECHNICAL UNIVERSITY

BY

ÖZGÜR ALTINOK

IN PARTIAL FULFILLMENT OF THE REQUIREMENTS
FOR
THE DEGREE OF MASTER OF SCIENCE
IN
PHYSICS

JULY 2011

Approval of the thesis:

HIGH-SPEED AUTOMATIC SCANNING SYSTEM FOR EMULSION ANALYSIS IN THE OPERA EXPERIMENT

submitted by **ÖZGÜR ALTINOK** in partial fulfillment of the requirements for the degree of **Master of Science in Physics Department, Middle East Technical University** by,

Prof. Dr. Canan Özgen _____
Dean, Graduate School of **Natural and Applied Sciences**

Prof. Dr. Sinan Bilikmen _____
Head of Department, **Physics**

Prof. Dr. Ali Murat Güler _____
Supervisor, **Physics Department**

Examining Committee Members:

Prof. Dr. Ramazan Sever
Physics Department, METU _____

Prof. Dr. Ali Murat Güler
Physics Department, METU _____

Assoc. Prof. Dr. Korkut Okan Ozansoy
Physics Engineering Department, Ankara University _____

Prof. Dr. Altuğ Özpineci
Physics Department, METU _____

Prof. Dr. Bayram Tekin
Physics Department, METU _____

Date: _____

I hereby declare that all information in this document has been obtained and presented in accordance with academic rules and ethical conduct. I also declare that, as required by these rules and conduct, I have fully cited and referenced all material and results that are not original to this work.

Name, Last Name: ÖZGÜR ALTINOK

Signature :

ABSTRACT

HIGH-SPEED AUTOMATIC SCANNING SYSTEM FOR EMULSION ANALYSIS IN THE OPERA EXPERIMENT

Altınok, Özgür

M.S., Department of Physics

Supervisor : Prof. Dr. Ali Murat Güler

July 2011, 63 pages

The aim of the OPERA experiment is to verify the neutrino oscillation, directly measuring the appearance of ν_τ from an initially pure ν_μ beam produced at CERN. For this purpose OPERA detector is located underground Gran Sasso Laboratory(LNGS) 730 km away from CERN. The detector structure designed to be a hybrid system consisting of emulsion targets and electronic detectors. Total area of the emulsion targets in the OPERA detector is around 110000 m^2 which needs fast and reliable automatic scanning systems. For this purpose, two different automatic scanning systems were developed in Japan and Europe. For now there are 12 scanning laboratories dedicated to the OPERA Experiment. The Emulsion Scanning Laboratory in the Physics department of METU is one of the scanning laboratories for the OPERA Experiment. The automatic scanning system in METU is European type which is using commercial hardware for easy construction and maintain. Also the laboratory has a unique feature in terms of experimental high energy physics laboratories. The emulsion scanning laboratory in METU is the first high energy laboratory in Turkey for data taking and data analysis at the same time. This M.S. thesis reports the successful installation and tests of the Automatic Scanning System in METU.

Keywords: Neutrino Oscillation, OPERA Experiment, Nuclear Emulsion, Automatic Scanning System

ÖZ

OPERA DENEYİNDE NÜKLEER EMÜLSİYON ANALİZİ İÇİN YÜKSEK-HIZLI OTOMATİK TARAMA SİSTEMİ

Altınok, Özgür
Yüksek Lisans, Fizik Bölümü
Tez Yöneticisi : Prof. Dr. Ali Murat Güler

Temmuz 2011, 63 sayfa

OPERA Deneyinin amacı nötrino salınımlarını, CERN'den gönderilen ve başlangıçta saf ν_μ hüzmesin de ν_τ oluşumunu direk olarak gözlemleyerek ispatlamaktır. Bu amaç için OPERA dedektörü Gran Sasso Laboratuvarlarında(LNGS) yerin altında, CERN'den 730 km uzaklığa kurulmuştur. Dedektör yapısı hem emülsiyon hedefi hem de elektronik dedektörleri kapsayacak şekilde dizayn edilmiştir. OPERA dedektöründe kullanılan toplam emülsiyon hedef alanı yaklaşık olarak 110000m^{2}dir, bu geniş alanı taramak için hassas tarama sistemlerine ihtiyaç duymaktadır. Bu amaç için, iki farklı otomatik tarama sistemi Japonya ve Avrupa'da geliştirilmiştir. Şimdilik OPERA deneyi için çalışan 12 farklı tarama laboratuvarı mevcuttur. ODTÜ Fizik Bölümündeki, Emülsiyon Tarama Laboratuvarı OPERA Deneyinde kullanılan laboratuvardan birisidir. ODTÜ'de mevcut olan otomatik tarama sistemi, Avrupada geliştirilen tarama sistemi türüdür. Ayrıca bu laboratuvar, deneysel yüksek enerji fiziği laboratuvarları arasında eşsiz bir özelliğe sahiptir. ODTÜ'de bulunan emülsiyon tarama laboratuvarı aynı anda veriyi alıp ve işleyen Türkiye'deki ilk ve tek deneysel yüksek enerji laboratuvarıdır. Bu Yüksek Lisans tezi, ODTÜ'deki Otomatik Tarama Sisteminin başarılı bir şekilde kurulumunun ve test sonuçlarının raporudur.

Anahtar Kelimeler: Nötrino Salınımları, OPERA Deneyi, Nükleer Emülsiyon, Otomatik Tarama Sistemi

This thesis is dedicated to my fiancée Esra Korkut...

ACKNOWLEDGMENTS

The work presented in this thesis would not have been possible without the involvement of a number of people. I would like to thank the following people in particular:

First of all, I would like to thank to my supervisor Prof. Dr. Ali Murat GÜLER for giving me an opportunity to involve in the OPERA Collaboration, and endless support and guide during my studies.

I would like to thank to Cristiano Bozza for his help on this work, without his precious efforts completing this study would be impossible.

Serhan Tufanlı deserves my deepest gratitude for everything he thought me, without his guidance and friendship I would not be in this position.

I would like to thank all METU OPERA Group members for their support in this study, namely: Mustafa Kamışcıoğlu, Behzad Hosseini, and Navid Hosseini.

Deniz Bender accompanied me in the long data taking sessions, I am very glad for his support and friendship.

I would like to thank all the people in Gran Sasso Scanning Laboratory for their teachings and support.

A special thanks for the Technical Staff in Department of Physics for their help in mounting the microscope in our laboratory.

I would like to thank to my fiancée Esra Korkut for standing next to me all the time.

I would like to thank to INFN for the financial support during my stays in LNGS, also to TUBITAK for 1 year financial support in this study.

Finally thanks to my family and all of my friends for their endless support and believe in me.

TABLE OF CONTENTS

LIST OF TABLES

TABLES

LIST OF FIGURES

FIGURES

CHAPTER 1

Introduction

In these years, human race is pursuing a great effort to understand the universe. There are lots of questions about the universe and its history: “How the all things we know started?”, “How the universe is evolving?”, “What will happen to universe in future?” or simply only one question, “What is the universe?”. These questions tried to be answered from the beginning of the known history. In different parts of the history, different universe models are proposed. For instance, some of the models were earth centered, assuming the earth is standing on the middle of everyting, and today we know that the Earth is nothing but a tiny piece of an evolving universe.

Today, the scientists are aware that we are living in an evolving universe. The changing structure of the universe with time, creates new challenging questions to the scientists. The High Energy Physics has a key role in answering these questions. The particle physicists trying to understand the universe by observing the properties of the particles exist in the universe. Although, there are different types of particles with unique properties, there is a very special type which has the most interesting structure. These particles are the neutrinos, the ghostlike particles of the universe.

Neutrinos are the neutral leptons corresponding electron, muon and tau. In other words, there are three different neutrinos, ν_e, ν_μ and ν_τ all corresponds their charged counter parts: e, μ, τ with respectively. Neutrinos have extremely small masses and they are accepted as fundamental particles. Due to their extraordinary small mass and neutral charge, neutrinos can only interact with matter only through weak interactions. Due to neutrino interactions with matter only through weak interactions, and they travel almost with speed of light, they can provide unique information about particle creation and annihilation around the universe,

no matter the distance and the matter distribution between.

The history of the neutrino physics dates back to Chadwick(1914), who discovered the continuous spectrum of beta decays in Ra B+C = $^{214}Pb + ^{214}Bi$. The continuous beta spectrum gives us two possibilities: (i) energy conservation does not hold in the nucleus, or alternatively, (ii) a neutral and penetrating particle carries the missing energy. This second idea was postulated by Pauli in 1930. The second idea clearly states that the particle had to be neutral in order to preserve the conservation of charge and also the particle must have a very tiny mass. For these reasons, Fermi called this "invisible" particle as *neutrino* [1].

Detecting this "invisible" particle takes 25 years, the existence of neutrinos is proved by the observation of the following reaction:

$$p^+ + \bar{\nu}_e \rightarrow n + e^+$$

Clyde Cowan and Fred Reines performed this experiment in 1955 inside an underground laboratory, which is located under a nuclear reactor at Savannah River. The nuclear reactors provides a neutrino flux around $10^{13}\, neutrinos/cm^2/s$, and the target was water with $CdCl_2$ solution. After a neutrino interaction occurs: The positrons annihilate with electrons by the pair-annihilation process which produces two gamma-rays with an energy 0.5 MeV in opposite directions. On the other hand, the neutrons were detected by the help of $CdCl_2$ solution; due to the property of cadmium being a good neutron absorber. When cadmium absorbs a neutron, the following reaction occurs:

$$n + ^{108}Cd \rightarrow ^{109}Cd^* \rightarrow ^{109}Cd + \gamma$$

The excited state of cadmium emits a gamma ray which can be detected by the photomultiplier tubes. The detection for this gamma takes $5 \times 10^{-6}\, s$ after the e^+e^- pair-annihilation process, which is a good experimental result. In other words, a gamma pair plus another gamma detection with a $5\,\mu s$ delay is a remarkable result for proving the neutrino existence [2]. Figure 1.1 gives the schematic view of the experiment.

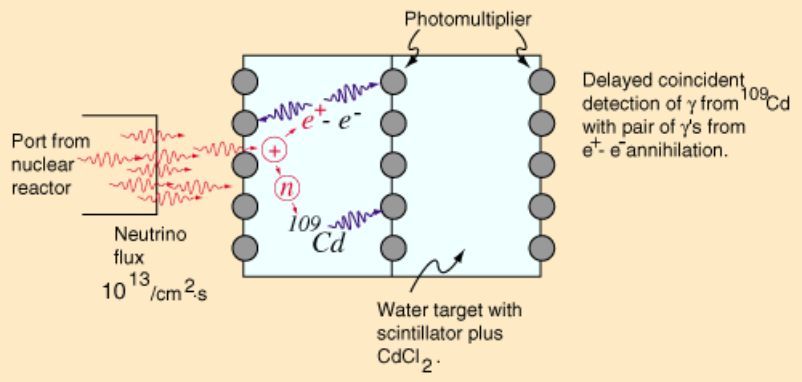

Figure 1.1: A schematic view of the Clyde Cowan and Fred Reines experiment [2].

Reines was awarded the Nobel Prize for this important discovery in 1995 [1].

After 7 years in 1962 the muon-neutrino is discovered by Leon Lederman, Melvin Schwartz and Jack Steinberger. The experiment conducted in Brokhaven National Laboratory and they used a beam consist of muons and muon-neutrinos, passing through a 5000 ton steel wall which stops the muons. Then finally, the pure neutrino beam enters neon-filled detector called a spark chamber. There, the impact of neutrinos on aluminum plates produced muon spark trails that could be detected and photographed which is proving the existence of muon-neutrinos. Also this experiment is the first one that uses a neutrino beam and these three scientists awarded a Nobel Prize in 1988 for their discovery of muon-neutrino [3].

Finally, the tau-neutrino is observed in Direct Observation of the NU Tau (DONUT) Experiment in Fermilab. The DONUT experiment used an intense beam of neutrinos, assuming the beam contains tau neutrinos as well, at a target consisting of iron plates with layers of emulsion plates sandwiched between them. The number of observed ν_τ charged current events in the experiment is 9, from a total of 578 observed neutrino interactions [4].

Once the existence of the neutrinos are proved experimentally, the scientists focused on the nuclear reaction mechanisms inside the stars by observing the neutrino flux coming from our sun. However, the scientists faced another problem with the predicted and observed rate of neutrino flux. The rate of the observed flux is lower than the predicted flux, this phenomenon called *Solar Neutrino Problem*.

The solar neutrino problem has forced the physicists to review their calculations and search

for new answers to explain the decreasing flux of ν_e created in the core of the Sun. One of the perspectives was revising the model that predicts the rate of the nuclear reactions in the Sun. On the other hand, some physicist proposed that the calculations was correct, but the ν_e created in the Sun, changed identity somewhere between the Sun and the detector. For example, a percentage of ν_es convert into other types of neutrinos (ν_μs or ν_τs), therefore, decreasing the flux of ν_e detected at the Earth [1]. The second idea known as Neutrino Oscillations and nowadays this phenomenon has been studied deeply by several experiments.

The OPERA experiment is one these experiments to verify the neutrino oscillation, directly measuring the appearance of tau-neutrino from an initially pure muon-neutrino beam produced at CERN. This thesis contains a dedicated work for the OPERA experiment.

The content of this thesis as follows: The next chapter, includes brief information about the phenomenology of neutrinos. The third chapter focuses on OPERA experiment, detector structure and final status of the OPERA experiment. In the fourth chapter, the structure and the working principle of the Automatic Scanning System is given. Fifth chapter includes the details on the fine-tuning of the microscope and preliminary scanning results.

CHAPTER 2

Phenomenology of Neutrinos

2.1 Standard Model

The so-called *Standard Model* that we use today is a theory which correctly explains the experimental data from high energy experiments. The theory was formulated by Glashow, Salam, and Weinberg (GSW) [5, 6, 7] in the 1960s to explain the properties of the particles and their interactions. According to the standard model, all matter is built from fundamental particles: quarks and leptons. Table 2.1 includes the list of the most fundamental particles:

Table 2.1: The most fundamental particles in Standard Model.

Particle	Flavor			Charge
Leptons	e	μ	τ	-1
	ν_e	ν_μ	ν_τ	0
Quarks	u	c	t	$2/3$
	d	s	b	$-1/3$

Likewise the leptons, the quarks also grouped into pairs: up and down, charm and strange, top and bottom. On the other hand, quarks can not exist as free particles, like leptons. They can be found only in different combinations, not as a free particle. This phenomenon is called as *quark confinement.*

Higgs boson is a proposal of Higgs mechanism [8] to explain how the matter become massive. Unlike the others, the Higgs boson has not been observed in high energy experiments. The existence of this boson is being investigated using the Large Hadron Collider (LHC) at CERN and the Tevatron at Fermilab.

The universe is mostly consist of stable particles, such as protons and electrons. We know that the protons and neutrons contain lightest u and d quarks, the particles consist of other heavier quarks such as s, c, b, t are heavier than the proton and neutron. These particles are unstable and decay rapidly($\approx 10^{-13}s$) to u, d combinations. Similarly, heavier leptons decay to electrons. Furthermore, these particles can only be observed in very high-energy collisions at particle accelerators or in cosmic rays.

In nature there are four types of fundamental interactions and these interactions occur by exchanging characteristic bosons.

Fundamental Interactions can be listed as:

Strong Interactions: This type of interaction is responsible for binding the quarks inside the particles and the neutrons and protons in the nuclei. This force is mediated by a massless particle, gluon.

Electromagnetic Interaction: All charged particles interact each other by electromagnetic interactions. Electrons are bounded to the atom by this interaction, and most importantly electromagnetic interaction governs the molecular formation in the universe. This force is mediated by photon exchange.

Weak Interactions: Most common type of this interaction is the nuclear β-decay, which is the emission of an electron and neutrino from the nucleus. There are two types of mediators for weak interactions: $W^{\pm}$ and Z^0

Gravitational Interactions: Gravitational interaction is the most standard interaction that occurs between all particles. On the atomic scale it is the weakest of the four fundamental interactions, but it dominates on universe scale. The mediator of gravitational interaction is supposed to be a graviton.

Following table summarizes the four fundamental interactions and their relative strengths:

Table 2.2: List of four fundamental interactions and their relative strengths [9].

Interaction	Mediator	Strength
Strong	gluon	1
Electromagnetic	photon	10^{-2}
Weak	$W^{\pm}, Z^0$	10^{-7}
Gravity	graviton	10^{-39}

2.2 Neutrino Interactions with Matter

As it is already stated the neutrino interacts with matter only through weak force, and this interaction is classified as Neutral Current (NC) and Charged Current (CC) interactions. NC interactions are mediated by the neutral Z bosons, and CC interactions involve the exchange of $W^+$and W^-bosons.

NC interactions are responsible for annihilation reactions involving neutrinos.

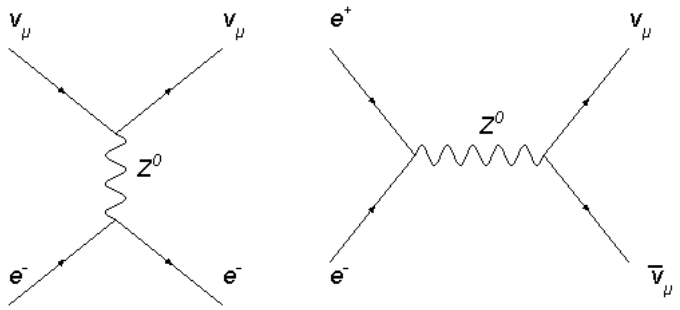

Figure 2.1: Feynman diagrams for NC interactions: $\nu_\mu + e^- \rightarrow \nu_\mu + e^+$ and $e^+ + e^- \rightarrow \nu_\mu + \bar{\nu}_\mu$ respectively.

In NC interactions neutrinos changes their energy by scattering with matter without any additional matter being created or annihilated. Such collisions are called *elastic scatterings* [1].

On the other hand, in the CC interactions there is an exchange of lepton. For instance, an antineutrino can be absorbed by a proton, which results of a neutron and a positron after the interaction.

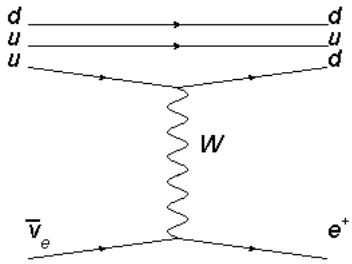

Figure 2.2: Feynman diagram for antineutrino absorption by a proton. One of the up quarks inside the proton, changes flavor to a down quark which transforms the proton to a neutron.

2.3 The Cross-Sections

Neutrino interactions involve the production of very high mass mediators, and this limits the neutrino interactions at low energies. In other words, "The matrix element of the interaction has a propagator term which includes the mass squared of the mediator particle:"

$$\frac{1}{q^2 - m^2_{mediator}} \tag{2.1}$$

where q is the momentum transfer of the reaction and the $m_{Z^0} \approx 91$ GeV and $m_W \approx 80$ GeV [1].

A crude calculation for the cross-section for a weak process: $\bar{\nu}_\mu \mu^- \rightarrow \bar{\nu}_e e^-$

The approximate expression for high-energy neutrino interactions with matter can be written as [1]:

$$\sigma \sim \frac{\alpha^2 s}{m_W^4} \sim G_F^2 E_{CM}^2 \tag{2.2}$$

where Fermi Constant $G_F = 1.1664 \cdot 10^{-5}\text{GeV}^{-2}$and E_{CM} is the center of momentum energy of the incoming neutrino [1].

$$\sigma_{weak} \sim 5 \cdot 10^{-44} \left(\frac{E_{cm}}{1MeV}\right)^2 cm^2 \tag{2.3}$$

For experimental purposes, expressing this result in terms of laboratory energy is helpful.

In a target experiment designed to detect the neutrino interactions in a general form: $\nu_x e^- \rightarrow \nu_x e^-$ and assume that the neutrino beam (ν_x) has a finite momentum targeted to a water tank in which the electrons have negligible velocities. The center of momentum energy squared, s, is the sum of the four-momenta of the colliding particles squared:

$$s = (P_e + P_\nu)^2 = [(E_e, \overrightarrow{p_e}) + (E_\nu, \overrightarrow{p_\nu})]^2 = [(m_e, 0) + (E_\nu, E_\nu \hat{p})]^2 \tag{2.4}$$

where $\left|\overrightarrow{p}\right| = E$ in natural units (c=1)

Therefore, in the laboratory frame:

$$s = 2m_e E_\nu + m_e^2 \tag{2.5}$$

For very high neutrino energies, ($E_\nu \gg m_e$), the last term can be neglected, and finally the cross-section of the neutrino interaction in laboratory frame:

$$\sigma(\nu_x e^- \rightarrow \nu_x e^-) \approx 2G_F^2 m_e E_\nu \tag{2.6}$$

From this relation, we can conclude that the cross-section for neutrino interactions directly and linearly proportional with the incoming neutrino energy [1].

If neutrino energy is higher than 5 MeV, the numerical expression for total cross-section of the general case:$\nu_x e^- \rightarrow \nu_x e^-$ leads to the result:

$$\sigma_{TOT} = C_x \cdot 9.5 \cdot 10^{-45} \cdot \left(\frac{E_\nu}{1MeV}\right) cm^2 \tag{2.7}$$

where the $C_e = 1$ and $C_\mu = C_\tau = \frac{1}{6.2}$

"The cross-section is larger for electron neutrinos, as they can, unlike the other neutrino species, couple to the electrons in the target through both NC and CC interactions" [1].

2.4 Neutrino Oscillations

The most accepted theory for neutrino disappearance is called neutrino oscillations which was proposed by Pontecorvo [10] and Maki [11]. The flavor eigenstates (ν_e,ν_μ,ν_τ) can be represented as linear combinations of the mass eigenstates (ν_1,ν_2,ν_3).

$$|\nu_\alpha >_t = \sum_j U_{\alpha j} exp(-iE_j t)|\nu_j > \tag{2.8}$$

where α represent e, μ, τ; and U is unitary matrix.

Properties of neutrino oscillations can be understood by studying the explicit solution for two interacting neutrinos [12].

For two-flavor case:

$$U = \begin{pmatrix} cos\theta & sin\theta \\ -sin\theta & cos\theta \end{pmatrix} \tag{2.9}$$

where θ denotes the vacuum mixing angle.

Using Eq. 2.9 in Eq. 2.8 leads to:

$$\begin{pmatrix} \nu_e \\ \nu_\mu \end{pmatrix} = \begin{pmatrix} cos\theta & sin\theta \\ -sin\theta & cos\theta \end{pmatrix} \begin{pmatrix} \nu_1 \\ \nu_2 \end{pmatrix} \tag{2.10}$$

The time evolution of an electron-neutrino can be expressed as:

$$|\nu_e >_t = cos\theta exp(-iE_1 t)|\nu_1 > + sin\theta exp(-iE_2 t)|\nu_2 > \tag{2.11}$$

where $E_1$and $E_2$are the energies of two mass eigenstates with the same momentum p. Since the neutrinos have very small masses: ($m_i \ll E_i$)

$$E_i \approx p + \frac{m_i^2}{2p} \tag{2.12}$$

The probability of an electron neutrino remains as an electron neutrino again after a time t:

$$P(\nu_e \rightarrow \nu_e) = | < \nu_e | \nu_e >_t |^2 = 1 - sin^2(2\theta) sin^2 \left[\frac{1}{2} (E_2 - E_1) t \right] \tag{2.13}$$

Inserting Eq.2.12 into Eq.2.13 leads to:

$$P(\nu_e \rightarrow \nu_e) = 1 - sin^2(2\theta) sin^2 \left[\left(\frac{m_2^2 - m_1^2}{4E} \right) t \right] \tag{2.14}$$

where E is the energy of ν_e.

Therefore, the probability that the electron neutrino changes its flavor to a muon neutrino after a time t:

$$P(\nu_e \rightarrow \nu_\mu) = sin^2(2\theta) sin^2 \left[\left(\frac{m_2^2 - m_1^2}{4E} \right) t \right] \tag{2.15}$$

"From Eq. 2.15 and Figure 2.3 the probability function for flavor change oscillates with an amplitude given by $sin^2(2\theta)$ and oscillation frequency $\sim \Delta m^2 / E$ " [1].

The amplitude and oscillation length of the flavor oscillation are:

$$A = sin^2(2\theta) \tag{2.16}$$

$$L_\nu = \frac{4\pi E \hbar}{\Delta m^2 c^3} = 1.27 \left(\frac{E}{1 MeV} \right) \left(\frac{1 eV^2}{\Delta m^2} \right) \tag{2.17}$$

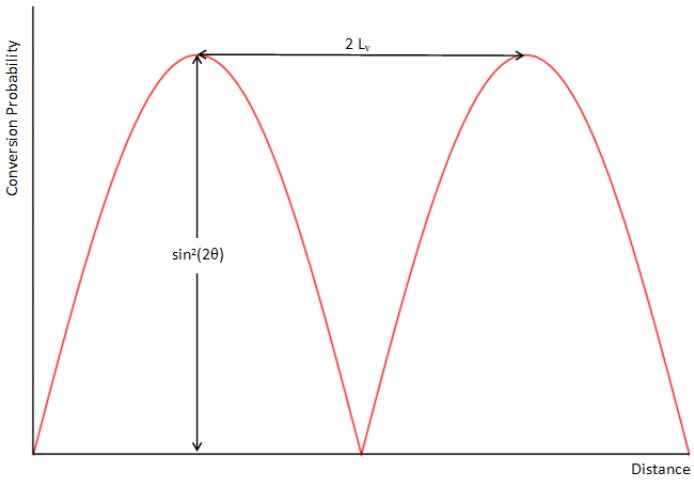

Figure 2.3: Probability distribution for $\nu_e \rightarrow \nu_\mu$

2.5 Neutrino Experiments

Due to the extremely low cross-section for neutrinos, the experiments need a very high flux of neutrino beams. Fortunately, stars are the main source of the neutrinos because of their nuclear reactions in the core. The main source of energy in hydrogen-burning stars (like our Sun) is through this mechanism:

$$4p + 2e^- \rightarrow^4 He + 2\nu_e + 26.731 MeV \tag{2.18}$$

where, the 2 percent (0.6 MeV) of the energy is carried by the neutrinos according to the standard solar model [1].

It is known that the Luminosity of the Sun equals 3.92×10^{26} Watts or 2.4×10^{39} MeV/s, according to the standard solar model, the Sun should emit 2×10^{38}electron neutrinos(ν_e) per second. If we calculate the neutrino flux on earth it becomes:

$$\phi_{\nu_e} = 6.5 \cdot 10^{14}\, m^{-2} s^{-1} \tag{2.19}$$

Due to this natural high flux, most of the experiments uses Sun as their neutrino source. Even with this huge flux, the extremely low cross-section makes the detection of neutrinos very

difficult. Several detection methods have been developed in different experiments.

Neutrino Absorption Experiments: These experiments mainly depend on the absorption of the neutrinos due to a specific nuclear reaction. For example the reaction $\nu_e + {}^{37}Cl \rightarrow {}^{37}Ar + e^-$ which is used in the experiment of Ray Davis group in the early 1960s [1]. The principal is extracting ${}^{37}Ar$ in chemical ways and counting the single atoms. The number of ${}^{37}Ar$ after the extraction of the background is equal to the number of electron neutrinos absorbed.

Neutrino Scattering Experiments: Neutrinos can undergo elastic scatterings with electrons, $\nu + e^- \rightarrow \nu + e^-$ after the scattering process, counting the scattered electrons gives the number of scattered neutrinos. In Japanese mine at Kamioka a large water tank and thousands of photomultipliers designed to detect scattered electron and hence find the number of incoming neutrinos. The principle was easy, as the water tank is stable in terms of any motion, electrons has no initial momentum. After the neutrinos scattered with the electrons, the recoiling electrons emit Cherenkov light, which can be detected by the photomultipliers. The number of total signal detected, is equal to the number of scattered neutrinos [1].

Although, the method of detection is usefull for describing the types of the experiments, the source of the neutrinos are also important to classify an experiment.

- Terrestrial Experiments
- Reactor Experiments
- Accelerator Experiments

In oscillation experiments, choosing the source of neutrinos is crucial, every type has its unique properties. For instance, in the reactor experiments, the $\bar{\nu}_e$ energies are so small (a few MeV). Even if a $\bar{\nu}_e \rightarrow \bar{\nu}_\mu$ oscillation happens, the charged current reaction $\bar{\nu}_\mu \rightarrow \mu$ is kinematically impossible. Therefore, the best oscillation signal in reactor experiments is disappearance of electron neutrinos as a function of distance from the source [1].

On the other hand, in the accelerator experiments ν_μ is created by a secondary beam. (For example: $\pi \rightarrow \mu\nu_\mu$). From the created ν_μ beam, the experiment is able to look for ν_e or ν_τ in an appearance mode which is the mode used in OPERA experiment.

2.5.1 Neutrino Oscillation Experiments

This section includes brief information for important neutrino oscillation experiments and their results.

- **The LSND and KARMEN Neutrino Oscillation Experiments**

  LSND experiment located at Los Alamos National Laboratory in United States performed an experiment with an 800 MeV high-intensity proton beam, and obtained an evidence for $\bar{\nu}_\mu \rightarrow \bar{\nu}_e$ oscillations with $\triangle m^2 > 0.2$ eV^2. On the other hand, KARMEN experiment used the same beam with LSND but no evidence for oscillations is observed. However, in the LSND experiment about 40 events were interpreted in terms of $\bar{\nu}_\mu \rightarrow \bar{\nu}_e$ oscillations [13].

- **The Super-Kamiokande Experiment**

  Super-Kamiokande detector is located in the Kamioka Mozumi mine in Japan. The detector is a cylindrical tank holding 50,000 tons of ultra-pure water. It is the largest water Cherenkov detector in the world designed to search for proton decay, study solar and atmospheric neutrinos. The experiment found the first evidence for atmospheric neutrino oscillations in 1998. The Super-Kamiokande measures the ratio of neutrino interactions to expected data.

  $$R \equiv \frac{(\mu/e)_{DATA}}{(\mu/e)_{MC}} \tag{2.20}$$

  For sub-Gev Ratio:

  $$R = 0.61 \pm 0.03(stat.) \pm 0.05(sys.) \tag{2.21}$$

  For multi-Gev Ratio:

  $$R = 0.66 \pm 0.06(stat.) \pm 0.08(sys.) \tag{2.22}$$

  where (μ/e) is the ratio of the number of measured neutrino interactions for muon and electron neutrinos respectively.

  Another most important outcome of the experiment for atmospheric neutrino oscillation mass parameter is given:

  $$\triangle m^2 = 2.5 \times 10^{-3}\, eV^2 \quad \theta = 45.0^\circ \tag{2.23}$$

If we check the 90% CL region, the result becomes:

$$1.9 \times 10^{-3}\, eV^2 < \triangle m^2 < 3.1 \times 10^{-3}\, eV^2 \quad \theta > 37.3^\circ \tag{2.24}$$

Along these important results, the Super-Kamiokande was the first experiment showing the neutrinos have mass and oscillating each other [13].

- **K2K: KEK to Kamioka Long-Baseline Neutrino Oscillation Experiment**

  The K2K experiment was the first long-baseline neutrino experiment operating at a distance 250 km away. The experiment used 12 GeV proton synchrotron accelerator at the High Energy Accelerator Research Organization (KEK) in Tsukuba city, targeted to the Super-Kamiokande detector [14]. The results of the K2K Experiment are consistent with the results of the Super-Kamiokande Experiment, which leads another evidence for neutrino mass. The reported result for the neutrino mass in K2K experiment is $\triangle m^2_{23} = 2.8 \times 10^{-3}\, eV^2$ at $\theta_{23} = 45.0^\circ$ which is in an agreement with the Super-Kamiokande Results [13, 15].

- **SNO: Sudbury Neutrino Observatory**

  Sudbury Neutrino Observatory results showed that the neutrinos oscillating each other, while they are travelling from Sun to Earth. The detector was built 6800 feet underground, in INCO's Creighton mine near Sudbury, Ontario, Canada [16]. The detector structure is designed with heavy water such that all flavors of neutrinos can be detected. Therefore, the SNO detector is able to compare the number of electron neutrinos and the number of other neutrinos. The latest results reported on mass parameter for two-flavor oscillations is $\triangle m^2_{12} = 7.59 \times 10^{-5}\, eV^2$ with $\theta_{12} = 34.4^\circ$ [17].

- **MINOS: The Main Injector Neutrino Oscillation Search**

  MINOS is a long-baseline neutrino experiment designed to search for neutrino oscillations in disappearance mode. MINOS uses two detectors, one located at Fermilab, at the source of the neutrinos, and the other located 730 km away, at the Soudan Underground Mine [18]. The data collected in MINOS have been analyzed and found to support the neutrino oscillation. They measured the mass square difference as $\Delta m^2_{23} = 2.32 \times 10^{-3}\, eV^2$and the mixing angle $\theta_{23} > 35.8^\circ$ (90% CL) [19].

- **The T2K Experiment**

The T2K experiment observes the ν_e appearance in a pure ν_μ beam. T2K uses a neutrino beam produced at J-PARC and directed 2.5° off-axis to Super-Kamiokande at a distance of 295 km. The T2K Collaboration reported their last results on June 13, 2011, as 6 events were passed the selection criteria with mass parameter as $|\triangle m^2_{23}| = 2.4\times10^{-3} eV^2$. They expect to see more events before concluding the ν_e appearance [20].

The results of the other experiments further encouraged the OPERA experiment to look for the neutrino oscillation evidence in an appearance mode. The details of the OPERA experiment will be given in the next chapter.

CHAPTER 3

OPERA Experiment

The OPERA (Oscillation Project with Emulsion-tRacking Apparatus) experiment is designed to investigate $\nu_\mu \rightarrow \nu_\tau$ oscillations by searching directly for ν_τ in an appearance mode within the CNGS[1] high energy beam. For this purpose, the OPERA experiment uses an hybrid detector consisting of Emulsion Cloud Chambers(ECC) and electronic detectors, which is located in LNGS[2] 730 km away from the neutrino source. In this chapter a detailed analysis of the CNGS beam and the OPERA detector will be given.

3.1 LNGS

The Gran Sasso National Laboratory (LNGS) is one of four INFN[3] national laboratories. It is an underground laboratory located 120 km away from Rome under Gran Sasso Mountain. Due to the large size of the Gran Sasso, 1400 m rock shields the LNGS, consequently reduces the cosmic muon flux to $10^{-6}/m^2/h$. This specialty makes it an ideal place for low background experiments such as OPERA experiment [21, 22]. LNGS located inside the longest road[4] tunnel in Europe between L'Aquila and Teramo as can be seen from Figure 3.1.

[1] CERN Neutrinos to Gran Sasso
[2] Laboratori Nazionali del Gran Sasso: The Gran Sasso National Laboratory
[3] Istituto Nazionale di Fisica Nucleare: National Institute of Nuclear Physics
[4] Two tunnels with an average length 10km each

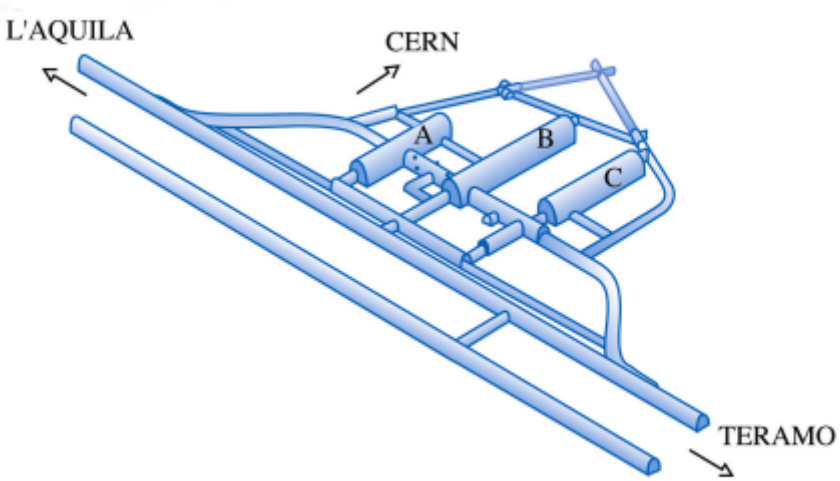

Figure 3.1: The OPERA detector located in Hall C and a Storage Room for extracted bricks is located in Hall B [23].

In addition to the underground facilities there is a building specially designed for OPERA experiment for developing the ECC Bricks after being extracted and a scanning station for changeable sheets is located on the surface.

3.2 The CNGS Neutrino Beam

The CNGS stands for "CERN Neutrino beam to Gran Sasso". A neutrino beam produced at CERN is directed towards the LNGS underground laboratory, 732 km away. From Figure 3.2 it can be seen that the layout of the apparatus to create the CNGS Neutrino beam.

A 400 GeV proton beam coming from the Super Proton Synchrotron (SPS) hits a target of 2 meters long graphite rods and produces secondary pions and kaons. The "Horn" and "Reflector" seen on Figure 3.2 are the magnetic lenses used to keep the pions and kaons in the beam line. The Helium bags are placed in between the Horn and Reflector and after the Reflector in order to reduce the interaction probability for secondary hadrons.

The pions and kaons will enter a 1 km long decay tube where the π^+ and K^+ decay producing μ^+ and ν_μ. At the end of the decay tunnel the remaining hadrons hit a huge block of carbon and

iron, which absorbs everything except the neutrinos and muons. The angle and the position of the beam can be measured by detecting the muons. For this purpose, two muon detector are included in the system [21, 24].

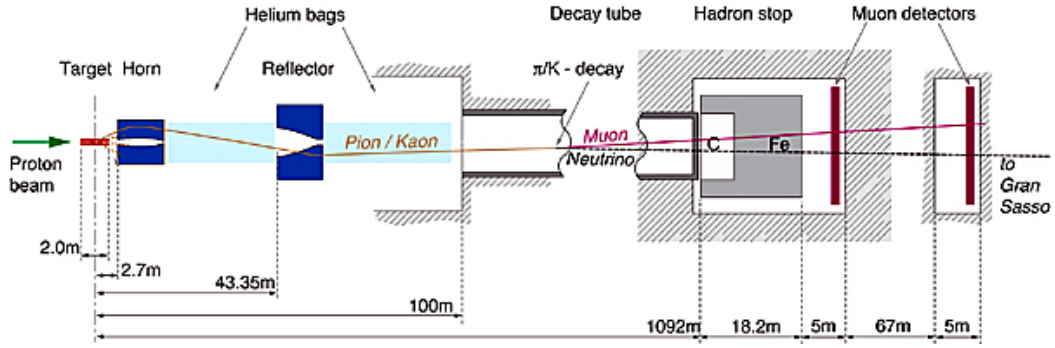

Figure 3.2: A detailed schemetics of the apparatus creating the CNGS Neutrino beam [25].

The neutrinos continue their way towards Gran Sasso with the trajectory seen in Figure 3.3, approximately in 1 km all the remaining muons are absorbed by the earth's crust. Calculations from the angle of the muons measured on muon detectors show that when the neutrino beam reaches Gran Sasso, it will have a diameter of about two kilometers.

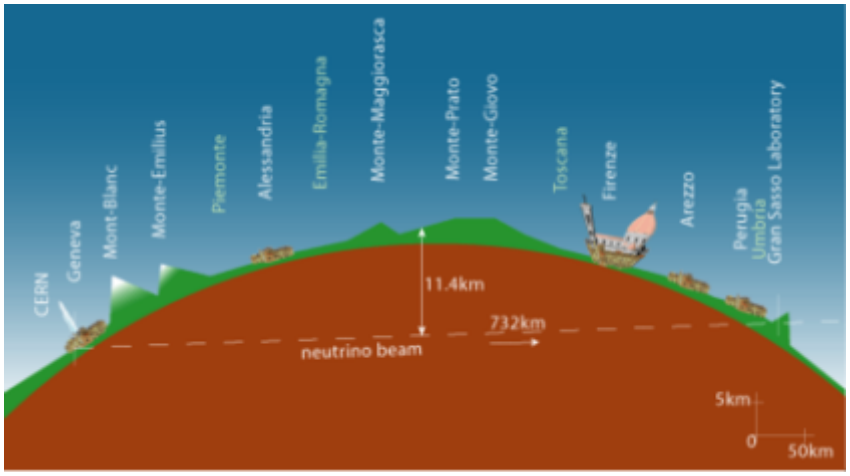

Figure 3.3: CNGS Trajectory from CERN to LNGS [26].

The intensity circulating in the SPS per cycle can reach 4.8×10^{13} protons, with an overall efficiency of 55% about 2.4×10^{13} protons can be expected. By assuming running time of 200 days per year it is estimated that 4.5×10^{19} protons can be delivered to the CNGS target per year[27].

3.3 OPERA Detector

The OPERA detector is an hybrid detector consisting of Emulsion Cloud Chambers(ECC), and electronic detectors, divided into two identical supermodules as seen on Figure 3.4. Each supermodule is formed as a target section followed by a muon spectrometer.

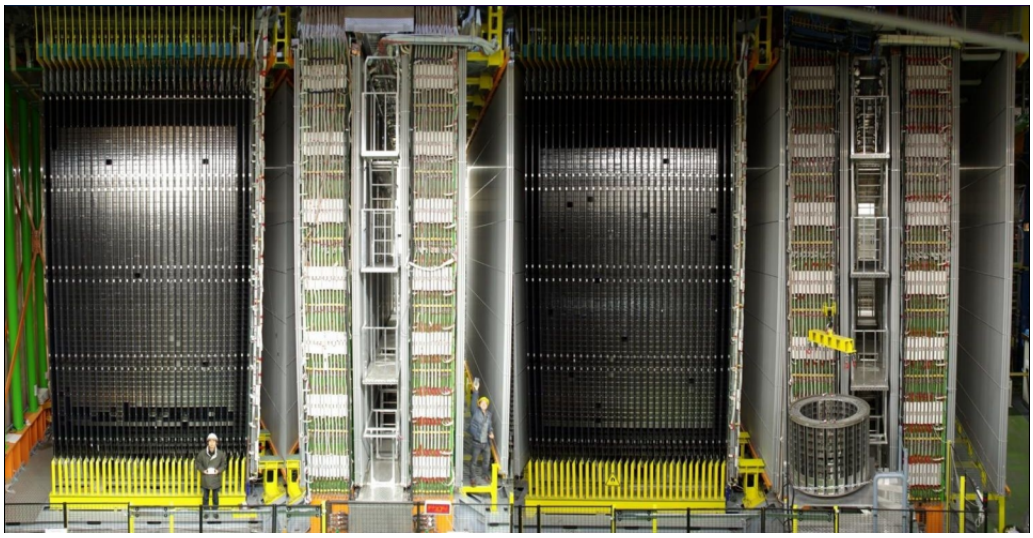

Figure 3.4: The two supermodules are visible, the black detectors are the Target Tracker and the Brick walls, and they are followed by the magnetic spectrometers. The Neutrino beam direction is left to right [28].

The target section is made of 31 brick walls sided with 31 Target Tracker (TT) planes. A close-up schematic view can be seen on Figure 3.5. Each wall consists of 3328 bricks and the whole target section on each Supermodule contains 103168 bricks equivalent to about 900 tons. Right after each brick wall TT walls are inserted, each target tracker contains 4 x 64 scintillator strips placed vertically as well as horizontally. The bricks consist of a lead/emulsion sandwich which provides both large target mass and high precision tracking of charged particles and the TT planes are used to determine the exact position of the brick which the neutrino interaction occurs [21, 24, 29].

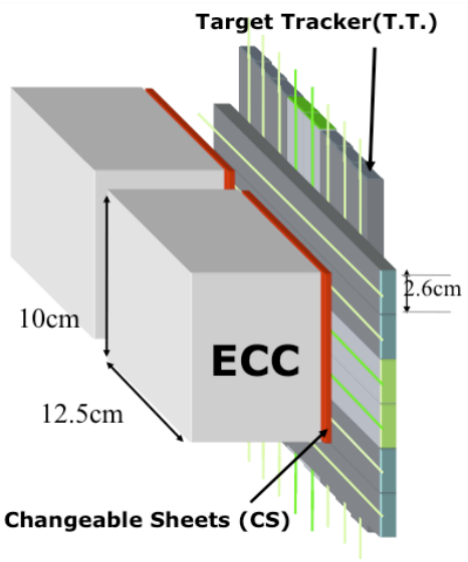

Figure 3.5: Schematic View of an ECC (OPERA Brick) sided with Target Tracker. The Neutrino beam direction is left to right [30].

The muon-spectrometers consist of dipolar magnets made of two iron walls sided by pairs of high resolution trackers. Each magnet is composed of 5 cm thick 2×12 iron slabs. A current of about 1.2 kA produces a magnetic field of 1.55 T in the iron. The main goals of the spectrometers are the muon momentum and charge measurements [21, 24].

3.3.1 Emulsion Cloud Chamber

The Emulsion Cloud Chamber(ECC) or so-called brick is a collection of 57 emulsion films and 56 1mm thick lead plates tightly packed with an aluminum cover. The detailed structure of a brick is shown on Figure 3.6. The bricks are the most fundamental element of the OPERA detector for two reasons:

1. Emulsion Films which are unique tools for identifying the particles with a low background. As the OPERA experiment based on detecting ν_τ appearance, it is crucial to detecting and identifying τ^- events in the experiment. Therefore, the usage of Emulsion Films provides valuable information for successfully identifying τ^- events in the detector.

2. In order to have a short radiation length, it is essential to have a massive detector. The

56 1mm thick lead plates provides high mass to a brick(8.3 kg) and the bricks with lead plates have a very high contribution to the total mass of the detector.

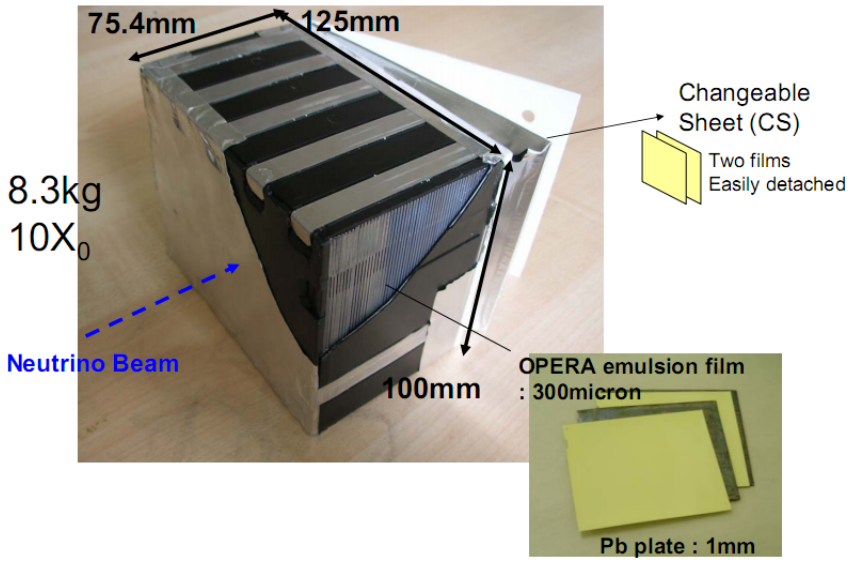

Figure 3.6: The detailed structure of an OPERA Brick [31].

The emulsion plates used in OPERA Bricks have two $\sim 45\mu m$ thickness emulsion layers on each side of a $\sim 200\mu m$ plastic base, in other words the emulsion films have $\sim 300\mu m$ total thickness.

The Changeable Sheet(CS) seen on Figure 3.6, determines whether the brick contains neutrino interaction or not. The CS is a pair of emulsions located inside a plastic box located back of the brick with respect to neutrino beam direction. The CS can easily removed from the brick and scanned without opening the whole brick. Since the CS is located back of the brick, it may contain information of a vertex inside the brick. CS scanning guides making the decision of scanning the whole brick, hence decreasing the workload of brick scanning. The detailed structure of a CS and an example of a passing through track can be seen on Figure 3.7.

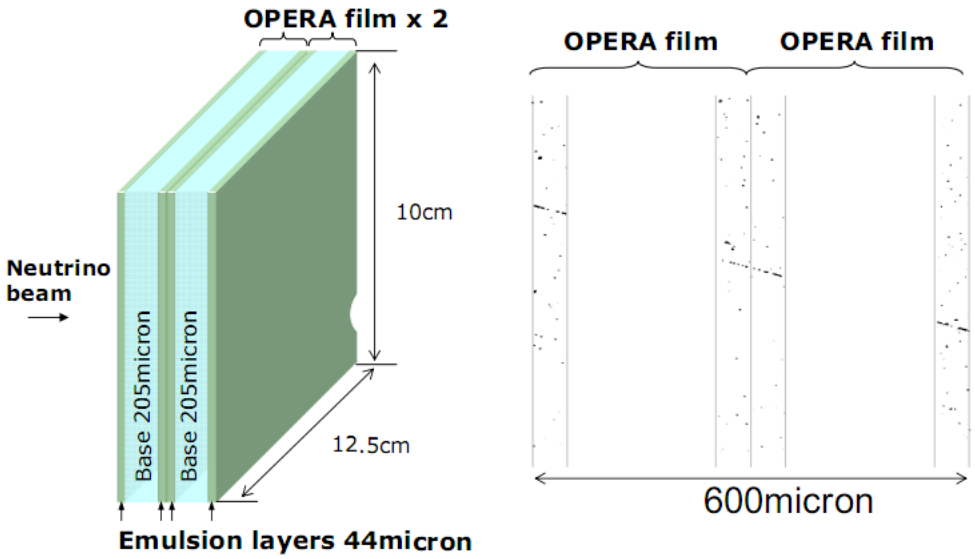

Figure 3.7: The detailed structure of a CS and an example of a passing through track [31].

3.3.2 Target Trackers

Target Trackers are electronic detectors placed behind of each brick wall in order to determine the brick where the neutrino interaction occurs. Target trackers combined with the CS gives a high resolution to select the correct brick. For this purpose, plastic scintillator strips read out by Wave Length Shifting (WLS) fibers have been chosen. Each brick wall is followed by two electronic tracker planes which provides 2D information (X and Y position) of the brick. The Figure 3.5, contains a detailed schematic of the Brick and Target Tracker relation.

An electronic target tracker module consists of two planes of 6.6 meters long scintillator strips in each transverse directions. The strips, 2.6cm wide, 1cm thick and all of them is connected to a 64 multi-anode photomultiplier tube via WLS fibers. An electronic target tracker module can be seen on Figure 3.8.

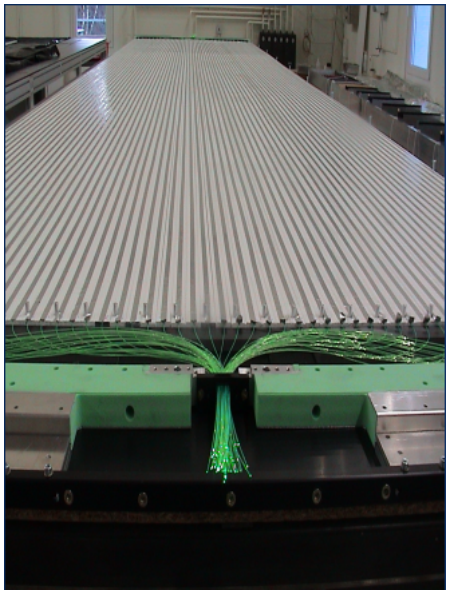

Figure 3.8: An electronic target tracker module in construction site [30].

Identifying the brick which includes the neutrino interaction called as Vertex Brick Identification. Vertex Brick Identification efficiency depends on whether the event has a μ^- in the final state or not. The vertex finding efficiency is 84%, with a 1.1 cm spatial resolution [29].

3.3.3 Muon Spectrometers

The main goals of the spectrometers are the muon momentum and charge measurements. The spectrometers used in the OPERA detector consist of active detectors (RPC, XPC and Drift Tubes) and a warm dipolar magnet made of two iron walls in between of pairs of high resolution trackers. Each wall is made of 12 iron plates 5 cm thick. The iron plates are magnetized using a current of about 1600 A circulating in the top and bottom copper coils creating a magnetic flux density in the tracking region 1.55 T with vertical field lines of opposite directions in the two magnet walls [24].

The high resolution trackers, denoted as Precision Trackers, consist of vertical drift tube planes with an overall resolution assumed as 0.5 mm in the bending direction. The two tracker planes housed between the two magnet walls provide an angular measurement of the track with a 100 cm lever arm. The lever arm for the external trackers is > 50 cm. This design leads to a momentum resolution better than 30% in the relevant kinematic domain [24].

The Inner Trackers are inserted between the magnet iron plates. They are made of RPC detectors. On each face of the chambers, the induced pulses are collected by 3 cm wide pickup copper strips in the horizontal and vertical directions. The Inner Trackers allow a coarse tracking inside the magnet to identify muons and make track matching between the Precision Trackers easier [24]. A detailed schematic of the muon spectrometer and a possible path of a muon inside the spectrometer can be seen on Figure 3.9.

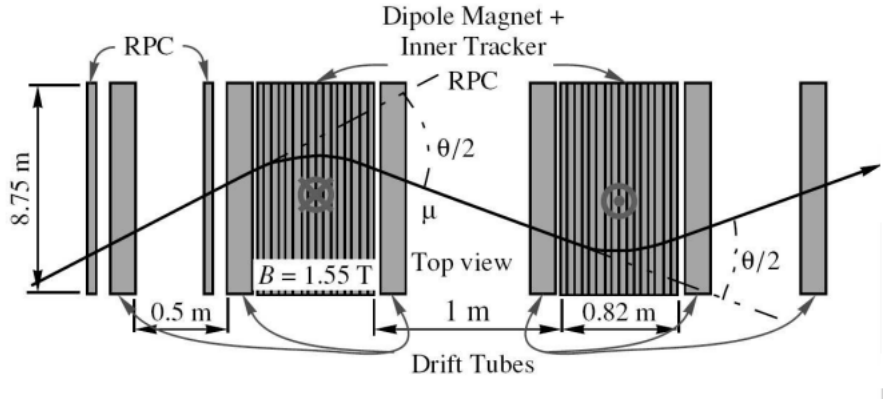

Figure 3.9: The Schematics of the Muon Spectrometer [21].

3.4 Nuclear Emulsions

Nuclear emulsions are the composition of micro-crystal silver halides (AgBr) with a gelatin layer. There is also variable quantity of water and a little glycerol in the chemical composition of emulsion. Emulsions in high energy physics are used for the 3-dimensional track recording of the charged particles. While a charged particle passes the emulsion media, it leaves a trial or an images that is know as *latent image*.

Latent image formation is the characteristic of AgBr. When light or a charged particle passes through the emulsion medium, it releases an electron and it turns silver ion to the silver atom. After a chemical development of emulsion, latent image became visible and 3-dimensional track of the charged particle is formed, which can be scanned automatically to retrieve the information.

In recent years, due to the development of automatic scanning systems, use of emulsions in the high energy experiments has increased. Modern scanning systems, allows scientists to use

large amount of emulsion targets in the experiments. The OPERA is the first experiment that uses a large area of nuclear emulsions which is about 110000 m^2.

3.4.1 OPERA Emulsion Plates

Since the required amount of emulsions is huge in OPERA, it is impossible to produce emulsions with previous techniques. Therefore, Fuji Company in Japan established an automatic production set up and all the emulsion films were produced in the commercial film production lines for the OPERA experiment.

In OPERA emulsion Plates there are two ~42μm thick emulsion layers and between them there is 210μm thick plastics base as can be seen in Figure 3.10. Also a 1μm thick protection layer was put over the emulsion layers in order to protect them from outer effects.

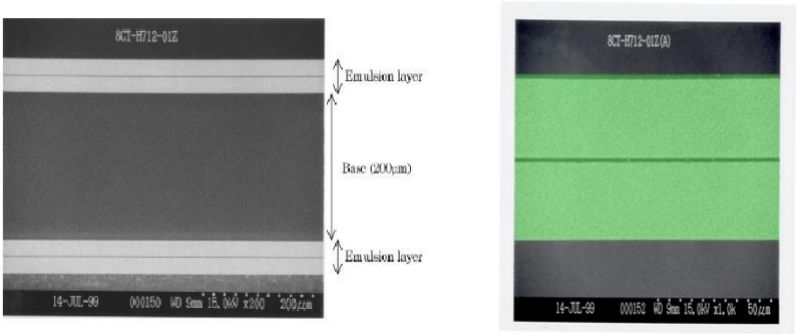

Figure 3.10: A microscopic view of the OPERA emulsion Plate [32].

Quality of the Emulsion Plates can be discussed in following titles:

Track Density Number of tracks grain per 100 μm. For the OPERA emulsion plates the *Track Density* is measured to be 35 $grains/100\,\mu m$ [32].

Fog Density Number of grains formed without a track in the 1000 μm^3 volume. For the OPERA emulsion plates *Fog Density* is expected to be $< 8\,grains/1000\,\mu m^3$ [32].

The other characteristics of the OPERA emulsion Plates is given in the following table:

Table 3.1: Properties of OPERA emulsion Plates [32].

density	$\rho = 2.4 g/cm^3$
average atomic number	$< A >= 18.2$
average atomic charge	$< Z >= 8.9$
radiation length	$X_0 = 5.5 cm$
$\left(\frac{dE}{dX}\right)_{mip}$	$1.55 MeV/g/cm^3$ or $37 keV/100 \mu m$
nuclear collision length	$\lambda_T = 33 cm$

3.5 Physics Performances

The OPERA experiment is designated to detect the $\nu_\mu \rightarrow \nu_\tau$ oscillation in an appearance mode. In other words, it is an appearance experiment which will detect ν_τ appearing in a pure ν_μ beam. The ν_τ appearance search is based on the observation of τ^- events produced by CC interactions, with the τ^- decaying in all possible decay modes:

$$\tau^- \rightarrow e^- \nu_\tau \bar{\nu}_e$$

$$\tau^- \rightarrow \mu^- \nu_\tau \bar{\nu}_\mu$$

$$\tau^- \rightarrow h^- \nu_\tau (n\pi^0)$$

$$\tau^- \rightarrow 3\pi \nu_\tau$$

Because of the expected event rate is small, it is crucial to efficiently separate the ν_τ CC events from all the other flavor neutrino events, and to keep the background at a very low level. For this purpose, the detectors will have to identify the event by exploiting the τ decay specific properties, which are short lifetime and the presence of missing transverse momentum due to the ν_τ in the final state [29].

3.5.1 Tau Decay Detection

The signal of the $\nu_\mu \rightarrow \nu_\tau$ oscillation is the CC interaction of ν_τ in the detector target is $\nu_\tau N \rightarrow \tau^- X$. After the produced τ^- will decay to either one of these: an electron, a muon or a single charged hadron. The branching ratios (BR) of the three decay modes are 17.8%, 17.4% and 49.5% for the electronic, muonic and hadronic channel, respectively [29]. Using the CNGS beam energy spectrum τ^- decay length distribution becomes as in Figure 3.11.

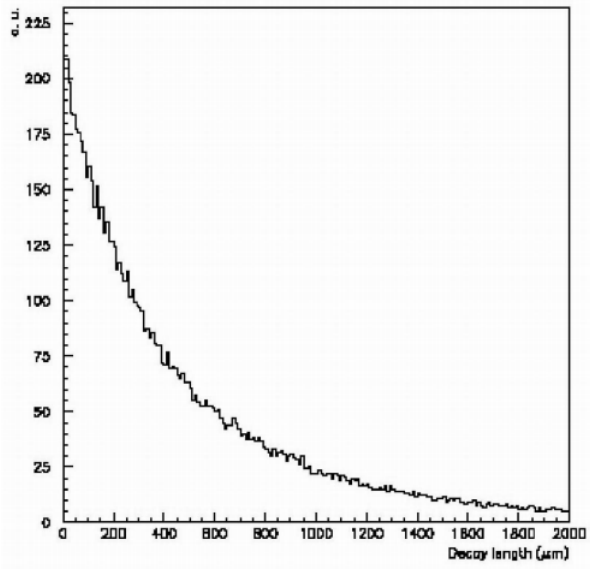

Figure 3.11: τ^- decay length distribution obtained assuming the CNGS energy spectrum [29].

When a τ^- produced inside a lead plate, due to a neutrino interaction. It will decay either within the same plate (*short decays*) or further downstream (*long decays*). Short decays are detected by measuring the impact parameter (IP) of the daughter track with respect to the tracks originating from the primary vertex, on the other hand for long decays the τ is detected by measuring the angle between the charged decay daughter and the parent direction. A schematic example of a long and short decay can be seen on Figure 3.12.

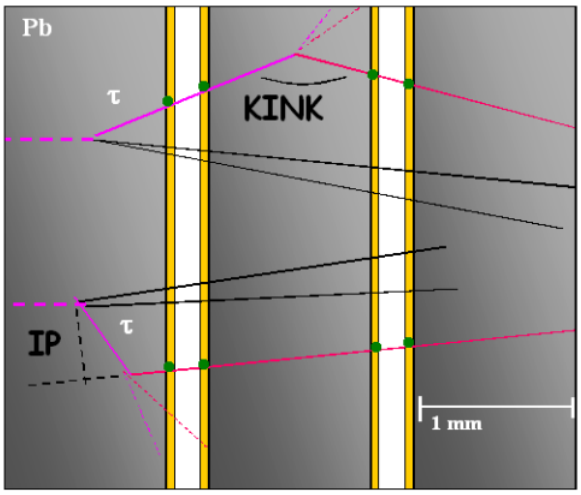

Figure 3.12: Schematic picture of the τ detection technique in the ECC cell for long (top) and for short (bottom) decays [24].

The detection of the τ decay to an electron has a unique property due to the dense brick design. Since the produced electrons creates electron showers inside the brick, the detection and identifying an energetic electron is possible. The density of the tracks in the constructed shower can be used to determine the energy of the electron.

If the τ decays to a muon, the produced muon will pass through all the detector from the vertex point to the spectrometer, leaving a trial in all the way on Target Trackers and the ECC's. In such and event locating the exact vertex position is relatively simpler. However, since the CNGS is a pure ν_μ beam, there is a potential background from large angle scattering of muons produced in ν_μCC interactions. This background can be reduced to an acceptable level by applying cuts on the kink angle and on the muon transverse momentum at the decay vertex. The energy of the muon can be calculated from the multiple scatterings in the lead plates and the momentum is measured in the muon spectrometers [24].

Finally, τ decays to an Hadron have the largest branching ratio but due to hadron interactions in the detector, there is a high background. For instance, one of the primary hadrons, can interact in the first lead plates and consequently it may simulate the τ decay. Strong kinematic cuts needed in order to reduce this background.

The τ decay detection efficiency could be estimated using four main steps:

1. Triggering system and brick finding

2. Vertex localization

3. Decay Type Detection

4. Kinematic Analysis of the decay

By taking account these four different steps, the efficiencies of τ detection for different decay modes are found as in Table 3.2.

Table 3.2: Summary of the τ detection efficiencies for different decay modes. Topologies: long and short. Type of events: Deep Inelastic Scattering (DIS) and Quasi Elastic Scattering (QE) [33].

Decay Mode	DIS Long (%)	QE Long (%)	DIS Short (%)	Total (%)
$\tau \rightarrow e$	2.7	2.3	1.3	3.4
$\tau \rightarrow \mu$	2.4	2.5	0.7	2.8
$\tau \rightarrow h$	2.8	3.5	-	2.9
Total	8.0	8.3	1.3	9.1

3.5.2 Background

There are four main background sources:

1. ν_τ production in the primary proton target in the CNGS

2. Decays of the charmed particles produced in the primary vertex

3. Large angle muon scattering

4. Hadronic reinteractions

All sources contribute their corresponding decay channel. The expected background for different channels for long and short decay modes can be seen on the following table.

Table 3.3: Expected signal and background for the different channels [33].

Decay Mode	Signal 1.2×10^{-3}	Signal 2.4×10^{-3}	Signal 5.4×10^{-3}	Background
$\tau \rightarrow e$ long	0.8	3.1	15.4	0.15
$\tau \rightarrow \mu$ long	0.7	2.9	14.5	0.29
$\tau \rightarrow h$ long	0.9	3.4	16.8	0.24
$\tau \rightarrow e$ short	0.2	0.9	4.5	0.03
$\tau \rightarrow \mu$ short	0.1	0.5	2.3	0.04
Total	2.7	10.8	53.5	0.75

3.6 Current Status of the OPERA Experiment

In OPERA experiment for a 5 years of data taking with an average CNGS beam intensity of 4.5×10^{19} proton on target (pot) per year and assuming a $\Delta m^2 = 2.5 \times 10^{-3} eV^2$ full mixing, **about 10 events are expected to be observed** [34]. When an interaction occurs inside the detector, a software reconstruction program finds the brick in which the neutrino interaction occur by processing the electronic detector data. In June 9, 2010, OPERA Collaboration published a paper reporting the observation of a first ν_τ candidate in OPERA experiment [35]. This section includes the details of this newest event.

3.6.1 Candidate Event Topology and Track Kinematics

The event is a decay of a τ into a charged hadron. For this decay these selection criteria applied for the primary and the secondary vertexes:

For the Secondary Vertex:

- the kink angle θ_{kink} must be larger than 20 mrad
- the secondary vertex must be within the two lead plates downstream of the primary vertex
- the momentum of the charged secondary particles must be larger than 2 GeV/c
- the total transverse momentum (P_T) of the decay products must be larger than 0.6 GeV/c, and also if there is no photon in the decay vertex, it must be 0.3 GeV/c

For the Primary Vertex:

- There must be no tracks belongs to a muon or an electron, since the track is expected to belong a tau.
- the missing transverse momentum ($P_T^{missing}$) must be smaller than 1 GeV/c
- the angle ϕ in the transverse plane between the τ candidate track and the hadronic shower direction must be larger than $\pi/2$.

These selection criteria were defined in the experiment proposal [36] and its addendum [37].

The event coordinate that fits these selection criteria located in 11^{th} wall of the first Super Module, and 3^{rd} brick from top, 24^{th} brick from left. A well centered position of the brick leads a detailed study of this event. In other words, the tracks of the event can be followed over large distances and secondary vertices including electromagnetic showers searched for in a large volume. For cross checking of the results, the event parameters is measured with European and Japanese scanning system separately. Measurements were consistent, and the averages are considered [35]. The event can be seen in Figure 3.13 and 3.14.

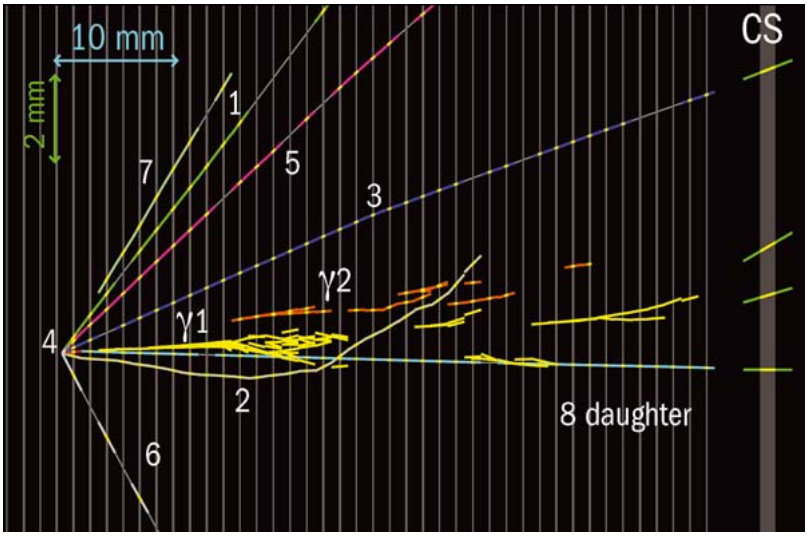

Figure 3.13: Longitudinal view of the event[38].

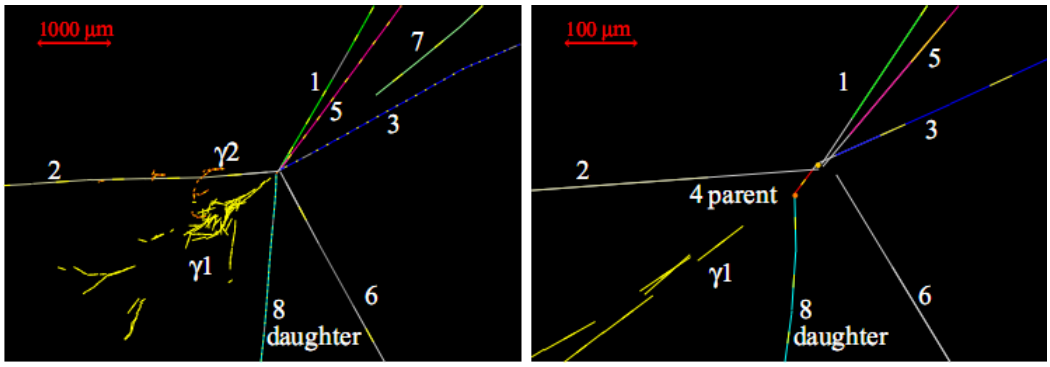

Figure 3.14: Left: Transverse view to the neutrino direction. Right: same view zoomed on the vertices[35].

As it is seen from the figures the primary neutrino interaction consists of 7 tracks and a visible

kink. Also two electromagnetic showers caused by γ-rays have been located near the event.

- Track 1 is left by a particle of momentum $0.78^{+0.13}_{-0.10}$ GeV/c. It is not found in the interaction brick immediately, it is reconstructed after the whole analysis.
- Track 2 is left by a heavily ionizing particle. From its residual range 32.0±0.5gcm^{-2} and the value of $p\beta = 0.32^{+0.31}_{-0.11}$GeV/c is measured and it is identified as a proton. Then the proton momentum resulting from the residual range corresponds to 0.60 ± 0.05GeV/c.
- Track 3 is left by a particle with a momentum $1.97^{+0.33}_{-0.25}$ GeV/c. Track 3 generates a two-prong interaction 4 bricks downstream of the primary vertex.
- Track 5 belongs to a particle with a momentum of $1.30^{+0.22}_{-0.16}$ GeV/c. Track 5 is followed in wall 12 also but it disappears in wall 13 after a total distance shorter than 174gcm^{-2}.
- Track 6 is identified as pion with a very low momentum $0.36^{+0.18}_{-0.09}$ GeV/c. The pion stops in the primary brick.
- Track 7 is not directly attached to the primary vertex and points to it with an $IP = 43^{+45}_{-43}\,\mu m$. Its starting point is separated from the primary vertex by 2 lead plates. Its origin is likely to be a prompt neutral particle, which is invisible in the emulsion. In the analysis, the momentum $0.49^{+0.29}_{-0.13}$ GeV/c has been added to the total momentum at the primary vertex.
- Track 4 clearly shows a kink topology with an angle of 41±2 mrad after a path length of 1335±35 μm corresponding a potential τ lepton. It is accepted as the parent track of a secondary interaction. Both the kink angle and the path length satisfy the selection criteria mentioned before.
- Track 8 is the kink daughter track, and it is left by a particle of a high momentum of (12^{+6}_{-3}) GeV/c which is expected to be above 2 GeV/c from the selection criteria. Track 8 IP with respect to the primary vertex is 55 ± 4 μm.

Also it is worth to mention that none of the tracks belongs to an electron or a muon. Also there are two different γ-rays exist in the interaction and their energies are calculated from the showers they created. The energies of $\gamma 1$ and $\gamma 2$ are (5.6±1.0(stat.)±1.7(syst.)) and (1.2±0.4(stat.)±0.4(syst.)) respectively.

The OPERA experiment reported the observation of a first ν_τ appearance candidate by giving a detailed picture of a τ^- lepton decay into $h^-(n\pi^0)\nu_\tau$ using the selection criteria reported [35]. With the expected number of events in 5 years of data taking being about 10, observing few more τ lepton decays inevitably leads to an experimental proof of neutrino oscillations in an appearance mode.

CHAPTER 4

The Automatic Scanning System in Ankara

4.1 Introduction

The photographic emulsion technique has been used in particle physics for many years. Manually inspecting and analyzing the films requires a huge amount of time and manpower. This limitation and the achievements in computer technology convinced research groups to develop an automatic scanning system for nuclear emulsion based experiments.

Automatic scanning system allows for fast extraction of physical information from emulsion sheets. If the number of emulsion plates used in the experiment is enormous like OPERA experiment, the automatic scanning system is the key factor to handle high amount of data in terms of quality and speed.

Nagoya University in Japan developed the first automatic scanning system for the CHORUS experiment in 1990s. The system called as *Track Selector* and it was designed to detect tracks with predicted angle in the field of view of a CCD camera. The track recognition algorithm completely implemented on the hardware, and the system is based on taking images at different positions on Z axis, and the tracks are extracted by shifting the images horizontally to find coincidences [39].

For the CHORUS experiment, European groups followed a different approach, Salerno Group developed an automatic scanning system based on multi-track reconstruction regardless of their slope. The purpose of this project was making use of the commercial products for both hardware and software. Also the flexibility of the software tracking algorithm, grants the user to easily upgrade and maintain the scanning system.

For the OPERA experiment both groups aim to improve their systems to catch up with high scanning speed needs of the OPERA experiment. In this section the properties of European Scanning System will be given.

4.2 European Scanning System Hardware

European Scanning System (ESS) is a specially designed apparatus with these properties:

- High performance mechanics with sub-micron position accuracy and very small settling time
- Optics with a sufficiently large field of view
- Camera with mega-pixel resolution and high frame rate
- Powerfull image processors

A layout of the ESS could be seen on Figure 4.1, as it is seen from the figure the fundamental parts of the ESS: A mechanical structure consist of three motorized axes, an optical part with light, a CMOS camera and finally a computer in order to control the axis movement and the processing the image. In the following chapters all these fundamental parts will be studied.

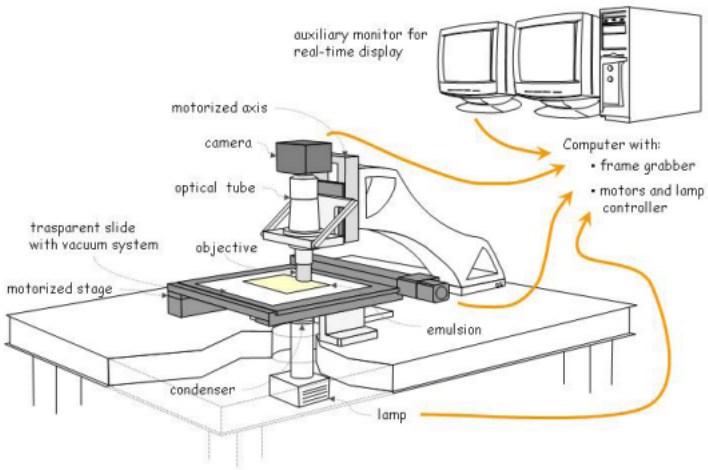

Figure 4.1: A Layout of European Scanning System [29].

4.2.1 Mechanical Structure

The ESS located in Ankara can be seen in Figure 4.2, the microscope is mounted on a high quality table which provides a vibration-free working environment. There are two different stages for 3 axis movement. Vertical stage[1], which is mounted to the granite arm, corresponds to the Z axis and the horizontal stage[2] corresponds to the X & Y axis. These stages are designed by the MICOS company in Germany. The most important parameters of these stages and the required parameters for our purposes are listed in the Table 4.1.

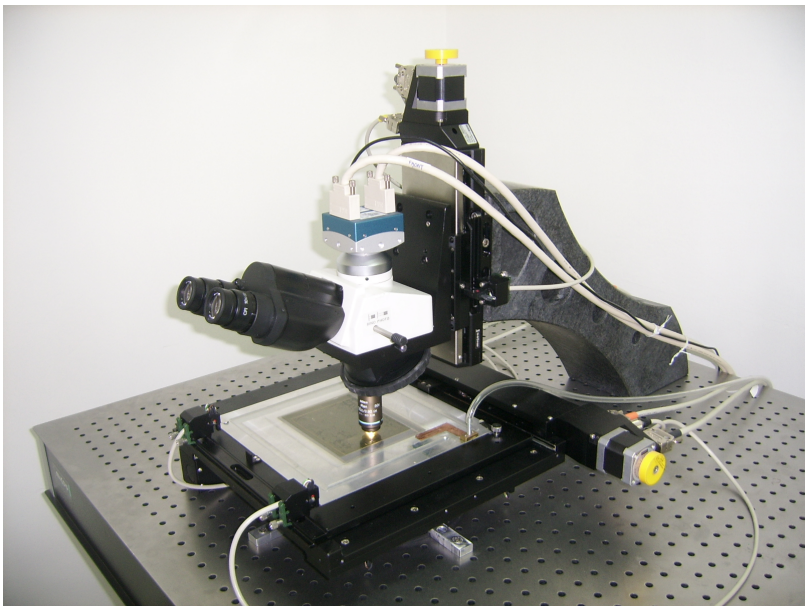

Figure 4.2: A photo of OPERA microscope in Ankara.

Table 4.1: Comparison of Stage Parameters and the ESS Requirements [40, 41].

MICOS MS-8 & LS-110	Parameters	Required Parameters
Travel Range (X & Y)	$205mm \times 205mm$	Maximum Scanning Area is $120mm \times 100mm$
Travel Range (Z)	$\gg 300\mu m$	Average OPERA emulsion Thickness is $300\mu m$
Maximum Speed	$45mm/s$	Affects the Scanning Speed
Position Accuracy	$\pm 1\mu m$	Affects the Scanning Accuracy

As it is clearly seen from the table, the stage range, speed and the accuracy parameters are perfectly matching for European Scanning System needs.

[1] MICOS LS-110
[2] MICOS MS-8

The stage movement is provided by a special type of motor designed by the Japanese company Vexta. A stepper motor, which is described below, is mounted on each axis in order to move the stages.

Stepper Motor "A stepper motor is a brushless, synchronous electric motor that can divide a full rotation into a large number of steps" [42]

The Stepper Motor[3] is one of the key element of European Scanning System which provides a movement on all axes in micrometer accuracy. These three motors are computer controlled using FlexMotion board provided by National Instruments.

The speed of the horizontal stage is one of the crucial points to obtain a suitable scanning speed. The speed and the acceleration of the movement have to be chosen in order to minimize the time needed to change the field of view. The horizontal displacements when changing field of view are $360\mu m$(X coordinate) and $280\mu m$ (Y coordinate). This is because the shape of the camera sensor is rectangular. Even the horizontal stage changes the field of view in a very high speed, still the system needs a settling time to focus the field. After several tests the optimized working conditions were set as:

$$Speed = 30\,mm/s$$

$$Acceleration = 200\,mm/s^2$$

for both X and Y Axes [24].

During data taking, the vertical stage moves at constant speed, in order to have equally spaced frames. The Figure 4.3 gives the details of the axes movement during data taking.

[3] 5 Phase Stepper - Motor RFK-545

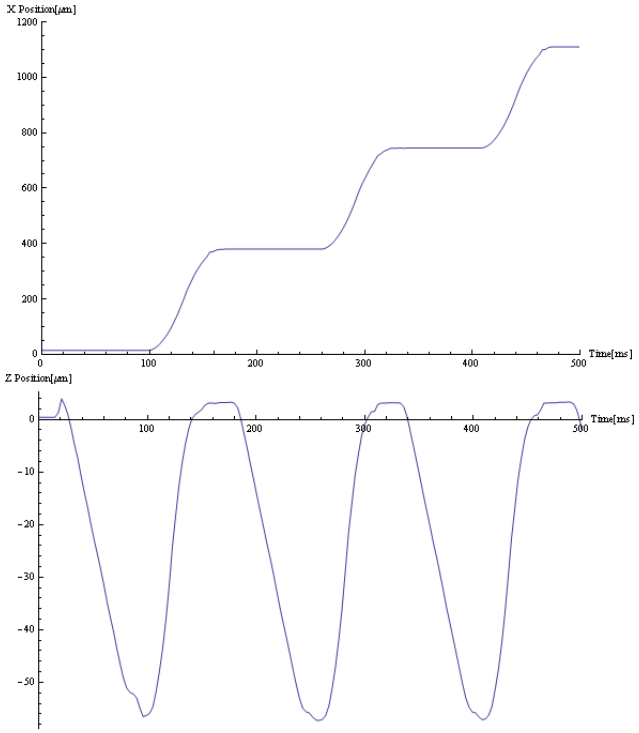

Figure 4.3: X axis movement on top and the Z axis movement on bottom during data taking simulation.

It is clearly seen from the figure, while data taking the X axes stays stationary and the Z axes moving in a constant speed taking frames at equal distances. When the scanning of one field is finished, the X axes go to next field meanwhile Z axes moves to the top of the emulsion plate and refocus for the new field. After focusing the scanning of the new field starts. It is important to note that this graph is an ideal simulation of ESS data taking session, normally the focusing on the each field may take more time.

4.2.2 Optical System

The Optical System can be analyzed in three main topics:

- Objective
- CMOS Camera
- Light System

Objective

The objective and the trinocular tube works together to focus the image to the surface of the CMOS camera. The optics are manufactured by the Nikon company and their working principle is based on the Nikon infinity optical system: The objective is designed in a way that the light emerging from the rear aperture is focused to infinity and a second lens located in the trinocular, forms the image at its focal plane which corresponds to surface of the CMOS camera.

The Nikon objective characteristics and the ESS requests can be seen on Table 4.2.

Table 4.2: Comparison of Nikon Objective Characteristics and the ESS Requirements [24].

Nikon CFI Plan Achromat 50x	Parameters	Required Parameters
Working Distance (WD)	$400\mu m$	Higher than $300\mu m$
Numerical Aperture (NA)	0.90	High as possible

The ESS objective is requested to have a *Working Distance (WD)* higher than $300\,\mu m$, in order to be able to scan both emulsion sides, and a *Numerical Aperture (NA)* sufficiently large.

Working Distance "The distance from the front lens element of the objective to the closest surface of the specimen is in sharp focus." [43]

Numerical Aperture "The numerical aperture of a microscope objective is a measure of its ability to gather light and resolve fine specimen detail at a fixed object distance." [44]

From the definitions, it is clear that the image quality is directly proportional with the Numerical Aperture of the objective. However, the other important factor on the image quality is reducing the diffraction of light when the light changing a medium. For this reason, ESS uses an *oil immersion objective*.

The oil immersion objective, uses oil as intermediate medium between emulsion and the objective front lens. In this way light rays passing through the emulsion sheet encounter an optically homogeneous medium because the refractive indexes of the crossed media are very similar ($n_{base} = 1.48$, $n_{emulsion} = 1.51 - 1.52$, $n_{oil} = 1.51$) [24].

The oil immersion objective used in European Scanning System can be seen on Figure 4.4.

Figure 4.4: A photo of the objective mounted to the microscope in Ankara

CMOS Camera

The camera mounted to the ESS is MC1310 from the Mikrotron company. It is a high-speed megapixel CMOS camera with Full Camera Link[4] interface. Unlike high resolution CCDs, modern CMOS sensors offer high resolution and extremely high data rates, which fits to the ESS needs. The CMOS sensor has 1280×1024 pixels, each having size of 12 μm (total sensor area is 1.5×1.2 cm^2). The camera is able to work up to a rate of 500 frames per second (fps) at full resolution, which implies a maximum data rate of 660 MB/s.

The ESS uses a camera configuration at 376 fps, which is satisfactory for the requested scanning speed. Also the selected exposure time for the ESS data taking is 1/6000 (about 0.17 ms).

The images are grabbed in a 256 level grey scale[5] and sent to the frame grabber in the controller PC. The frame grabber and the image processor are integrated in the same board: the *Matrox Odyssey Xpr*o produced by the Canadian Matrox company. After processing the image, the emulsion view appears on the ESS monitor as in the Figure 4.5.

[4] Camera Link is a new digital standard that sends back serialized data instead of parallel ones. [24]
[5] 0 = black, 255 = white

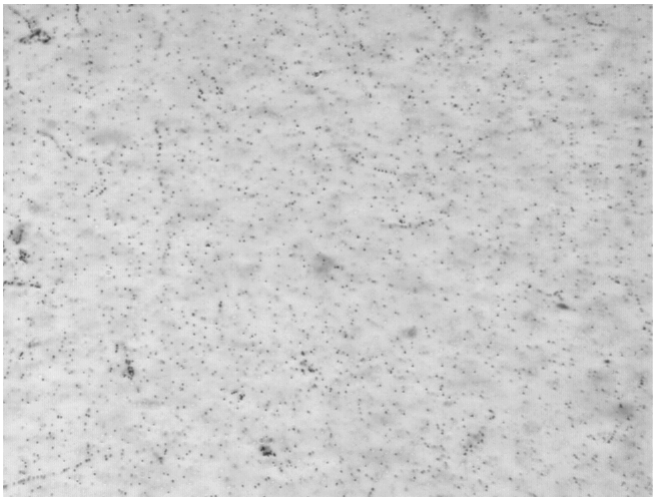

Figure 4.5: The Emulsion View seen on Ankara ESS monitor.

Light System

The light system was developed by Nikon-Italy after a joint R&D activity carried out in collaboration with the Napoli and Bari groups [24].

The light system uses a tungsten-halogen lamp that operates on a direct current and produces up to 100 watts power for illumination. The 12 volts lamp voltage is controlled by a power supply, connected to the motion control board, allows to change the brightness of the lamp using ESS software. The light from the lamphouse is directed into the microscope base through a collector lens, and then through a glass diffuser [24].

The power supply manufactured in Turkey can be seen on Figure 4.6.

Figure 4.6: A photo of the power supply in Ankara

4.3 European Scanning System Software

4.3.1 The SySal Software

The SySal software written by Cristiano Bozza from Salerno Group was developed on a Windows platform in the .NET framework by using the object-oriented C++ and C# languages. The SySal Software is written on a modular structure where each different object responsible for a well defined task. The main screen including all abjects can be seen on Figure 4.7.

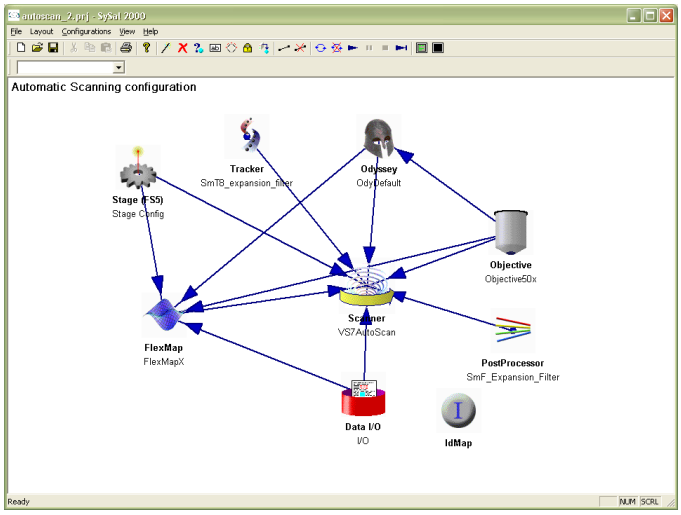

Figure 4.7: SySal Main Screen

The list and the tasks of the all objects can be listed as:

Objective stores the information related to the used objective and performs the pixel to micron conversion.

Odyssey drives the Odyssey board where the camera frame flux in handled and the clustering process is hold.

Stage(FS5) is interfaced to the stage controllers and set the movements of the three axes.

Tracker is responsible for track pattern recognition, recognizing sequences of geometrically aligned clusters.

PostProcessor performs the tracks fit.

Data I/O handles data Input/Output

FlexMap transforms coordinates and vectors from the current stage reference frame to the emulsion local reference system.

Scanner is the main module, which uses all the other objects to manage the scanning.

Using SySal the user can change the configuration of each object, Stage Config parameters is given as an example on Figure 4.8.

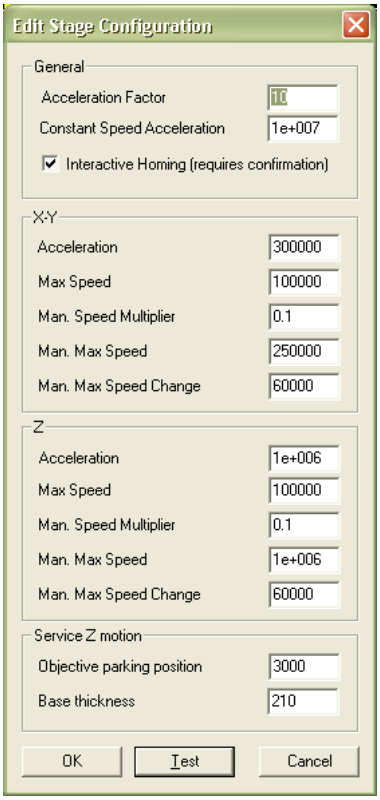

Figure 4.8: The *StageConfig* parameters accessed in SySal.

4.3.2 SySal Image Processing & Tracking

As it is mentioned in the ESS Hardware section during data taking, the emulsion is scanned view by view by the camera and the images are sent to the Odyssey board. In other words the readout is performed by moving the focal plane of the objective inside the emulsion layer with constant speed, and for each field of view a series of successive images are taken by the camera. This processes can be seen in Figure 4.9.

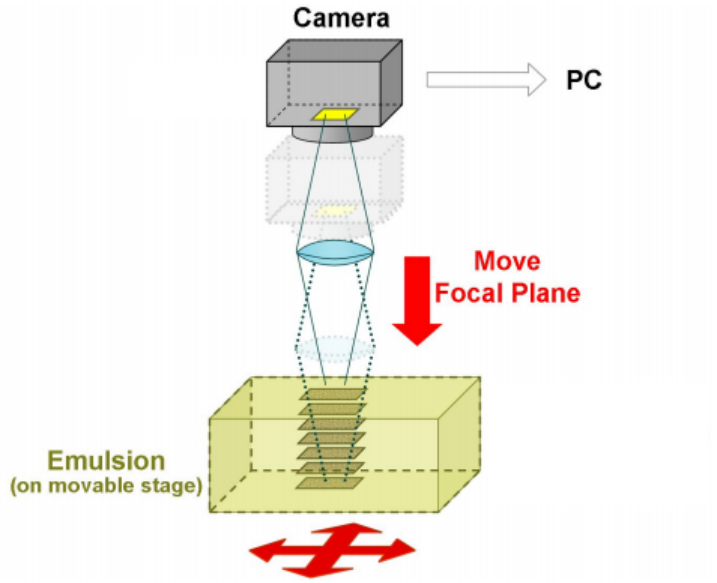

Figure 4.9: Camera is taking a series of successive images in different depths of the Emulsion [39].

After the images are sent to the Odyssey board the cluster search is performed. The first operation is the flat field subtraction. The flat field consist of one image taken without emulsion, the clusters appears on the flat field image generally the dusts on the camera sensor. By subtracting the flat field image from the real image, we remove the possibility of detecting the dust on the camera as a fake track.

Secondly digital images are analyzed for the recognition of the dark spots in the image. Some of these dark spots belongs to the tracks but most of the spots are not belonging to the tracks but they always exists in the emulsion. They are called as fog grains.

In order to make a selection between true tracks and the fog grains, a convolution filter is used. Convolution filter enhances the contrast between focused grains and background. An example of 3×3 high pass filter kernel:

-1	-1	-1
-1	9	-1
-1	-1	-1

Convolution is a local operation: the output value p_{ij} of the pixel at a specific coordinate is a

weighted sum of the input values of the neighborhood pixels, the weights w_{lk} are given by the filter kernel; for a 3x3 kernel:

$$p_{ij} = \sum_{l=1}^{3}\sum_{k=1}^{3} w_{lk} g(i+l, j+k)$$

where g is the grey level input value.

Then a well-chosen threshold is applied to extract the dark spots that are candidate to become grains; the pixels are divided in two classes: the ones with the filter response above threshold, whose values in binarized image are set to 0, are the ”white” pixels, and the ones with filter response below the threshold whose values are set to 1, are the ”black” pixels [39].

Third stage of the image processing is the clustering. Combining grains from different layers to recognize geometrical alignments. A sequence of aligned grains is called a *micro-track*. This process and an example of a micro-track can be seen on Figure 4.10.

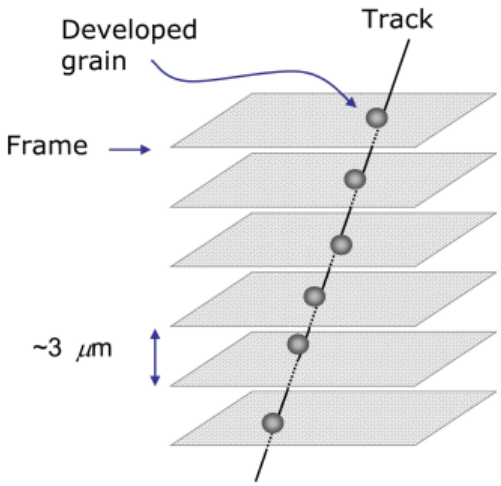

Figure 4.10: Clustering Process: Searching for aligned grains in different emulsion layers [29].

The final step is base-track reconstruction in which the micro-tracks on the top and bottom emulsion layers connected to form a base-track. The particle track position and slope is determined by a linear fit of base-tracks through the emulsions.

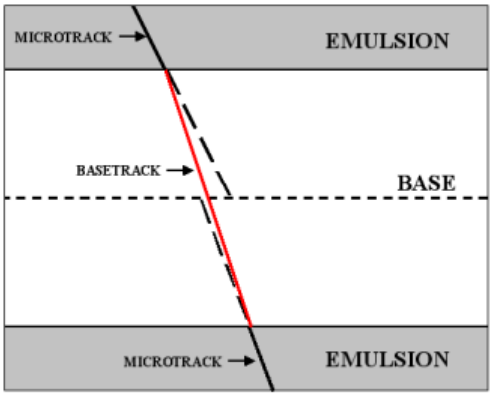

Figure 4.11: The principle of base-track reconstruction: the micro-tracks matching is obtained when an acceptable agreement in slope and position is found. The base-track is formed by joining the two points closer to the base [29].

CHAPTER 5

Test Scanning Results

5.1 Test Beam at CERN July 2007

In the beginning of the OPERA experiment, a test beam is exposed to a set of OPERA emulsion plates to study the tracking efficiency of the new scanning systems. In Ankara we have 8 plates from that exposure and the results reported in here based on these emulsion plates.

80 films were exposed with a uniform pion beam on a surface of 10×10 cm^2 . The angle distribution as measured is reported in Table 5.1.

Table 5.1: Details of the exposure for the sample at 10 GeV π [45].

Angle (mrad)	Triggers
0	53158
100	52910
-200	53136
300	53529
-400	53713
500	52914
-600	54029

Exposure on certain angles lets us to calculate the accuracy of the scanning system. Data taken from test emulsion plates can be compared with these parameters to understand the scanning system working as expected or not.

After several testing we realized that the quality and the thickness of the emulsion plates in the set were not equal. Therefore, most of the data taken with the plates having the best quality. We used the plate 37 and 38 for the accuracy and precision tests.

5.2 Optical Alignment of the Scanning System

In order to have a high accuracy and precision in the scanning system, we spent significant amount of time. The most important factor that affects the accuracy and the precision is optical alignment of the microscope. First alignment type is shown in Figure 5.1.

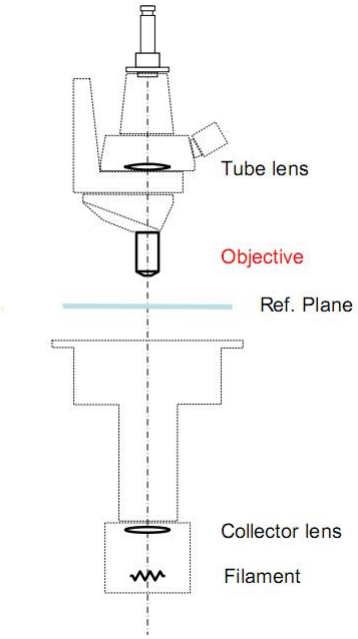

Figure 5.1: For the best image quality, all the parts must be well centered along the optical axis [46].

We managed to center all the optical components along the optical axis, and the results of the scanning and the image quality is significantly improved. The scanning results after the improvement will be given in the following sections. The Figure 5.2 shows the alignment of the optical axis when the condenser is almost closed.

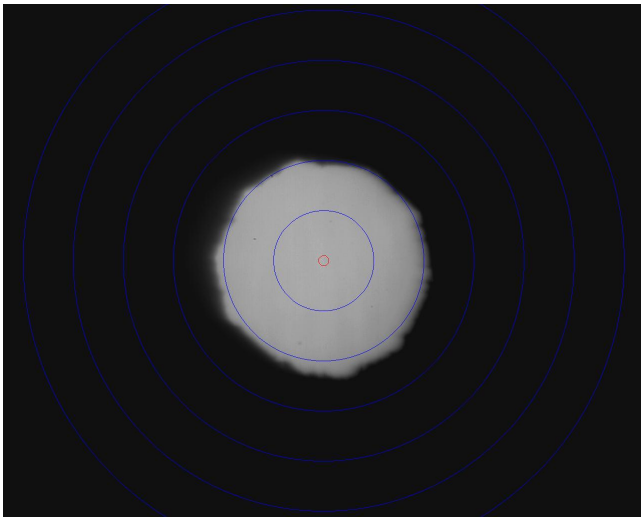

Figure 5.2: The Light is centered with the CMOS camera along with the other optical parts.

The optical centering is not the only parameter that affects the image quality, also any slant on X or Y axis may cause a misalignment leading to a lower image quality. The accepted axes on the microscope is shown in Figure 5.3.

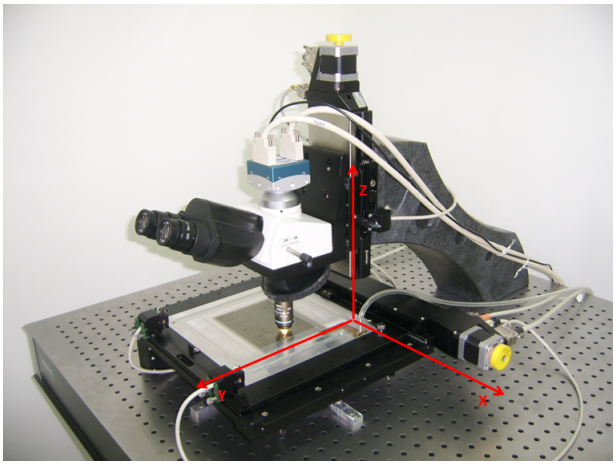

Figure 5.3: The axes as they seen on the microscope.

Having a slant on X direction is more probable than having a slant on Y direction. The reason is mounting styles: On Y direction the vertical stage is mounted directly to the granite arm, on the other hand the X direction is not limited on any sides which leads an extra degree of freedom. Due to the accuracy of the system expects the slant lower than a few miliradiants, using a physical tool to measure the slant is not possible.

We used a double scanning technique to measure the slant on X direction. For this purpose we used the test emulsion mentioned in the previous section. First we scanned the plate on normal orientation and than the plate is scanned as 180 degrees oriented. If there is a slant, we would see a difference on the slope of X. The results of the two scannings can be compared to check the slant. The results of measurements can be seen on Figure 5.4 and 5.5.

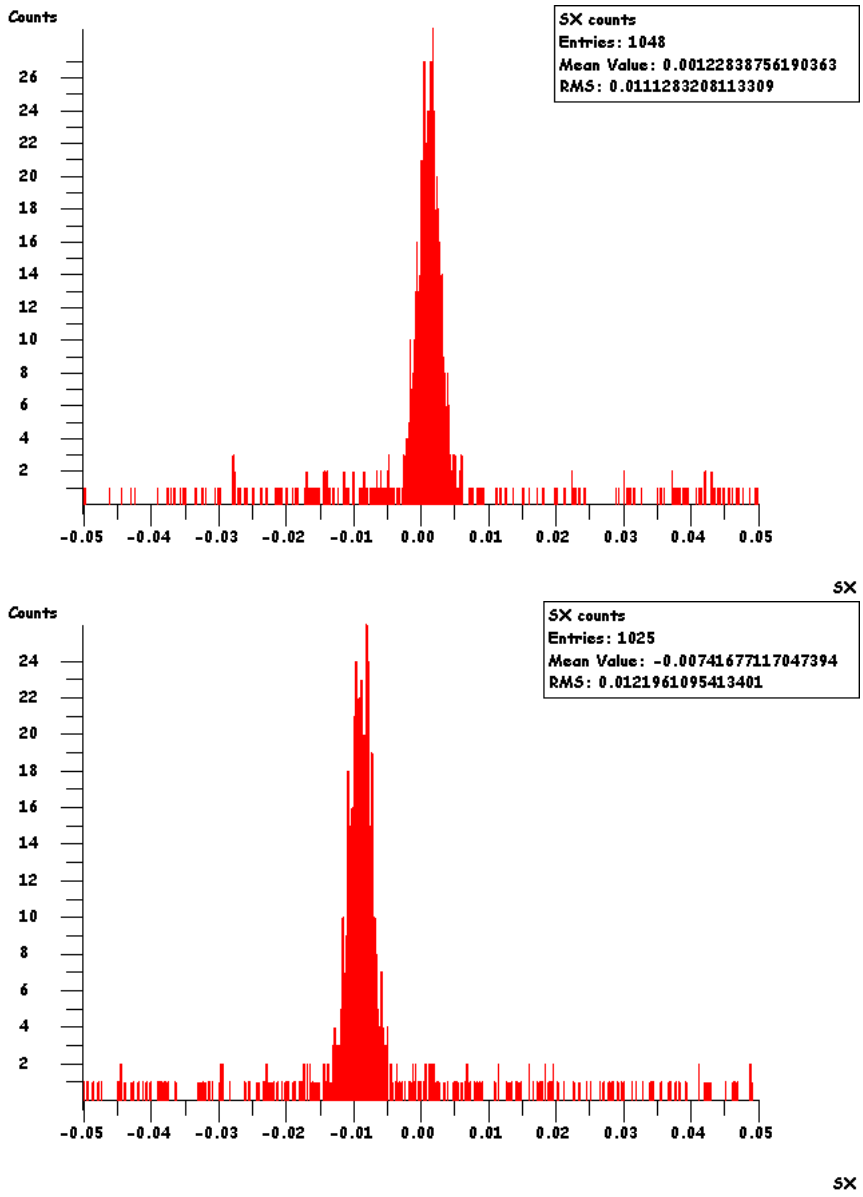

Figure 5.4: Slant measurement around the zero slope. Top: Normal orientation, Bottom: 180 degree orientation.

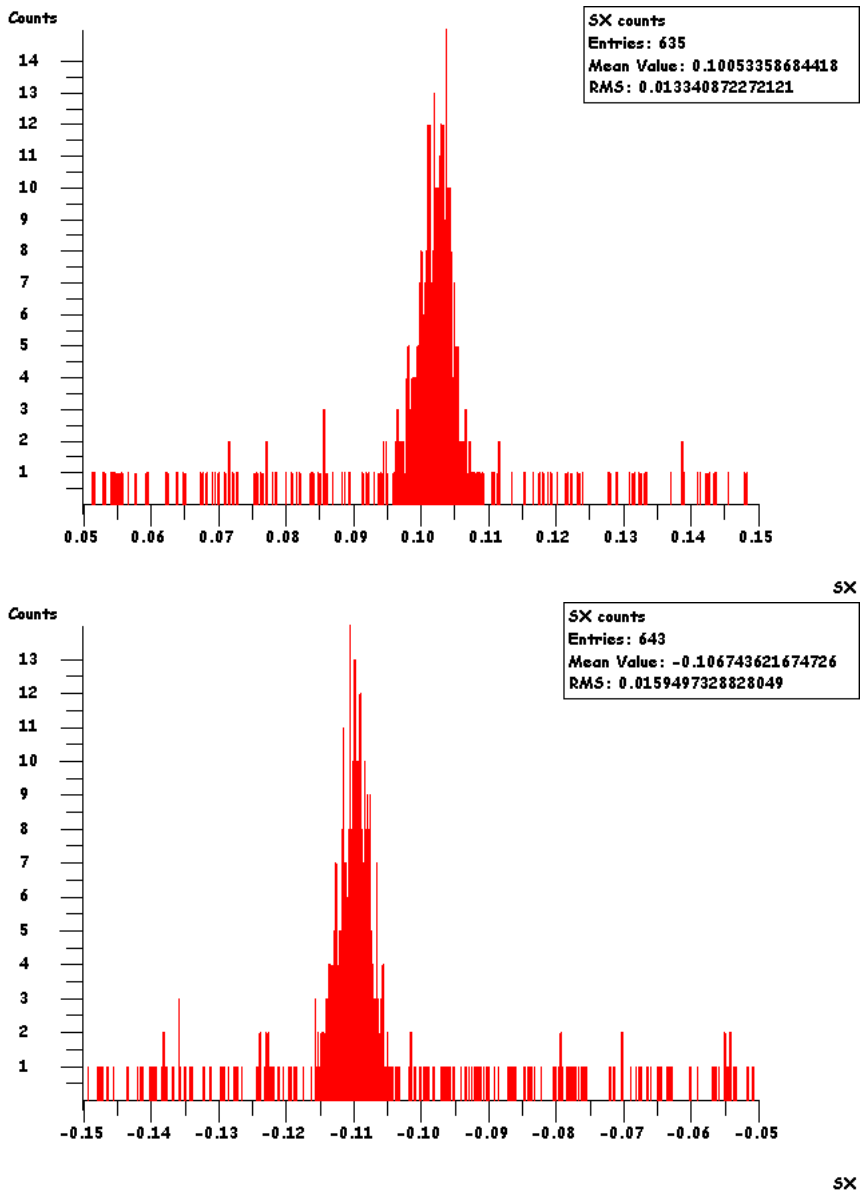

Figure 5.5: Slant measurement around the slope 10 mrad. Top: Normal orientation, Bottom: 180 degree orientation.

From the figures the slant of the system can be calculated as:

For the zero slope:

$$Slant = \frac{0.00123 - 0.00742}{2} \approx -3\,mrad \tag{5.1}$$

For the slope 10 *mrad*:

$$Slant = \frac{0.10053 - 0.10674}{2} \approx -3\,mrad \tag{5.2}$$

Slant on the optical axis is accepted to a critical value. The slant of the optical axis must not effect the working of the scanning system. For instance, if the slant is too much for the system to track the particle trails, this slant should be improved. The parameters inside the tracking and linking algorithm accepts a maximum slant of $6\,mrad$. Our results are $\approx 3\,mrad$ which is acceptable.

5.3 Performance Tests

In order to start data testing for the OPERA experiment, all newly automatic scanning systems must perform with high performance in terms of accuracy, precision and efficiency. The tests for each property was done and reported in this section.

5.3.1 Accuracy Test

For the accuracy of the system we compared our results with the Table 5.1. The number of incidents is related with the scanning area, we kept the scanning area as $1.5 \times 1.0\,cm^2$ and even with this small scanning area the results were satisfactory. Figure 5.6 and 5.7 report our results on slope of X direction.

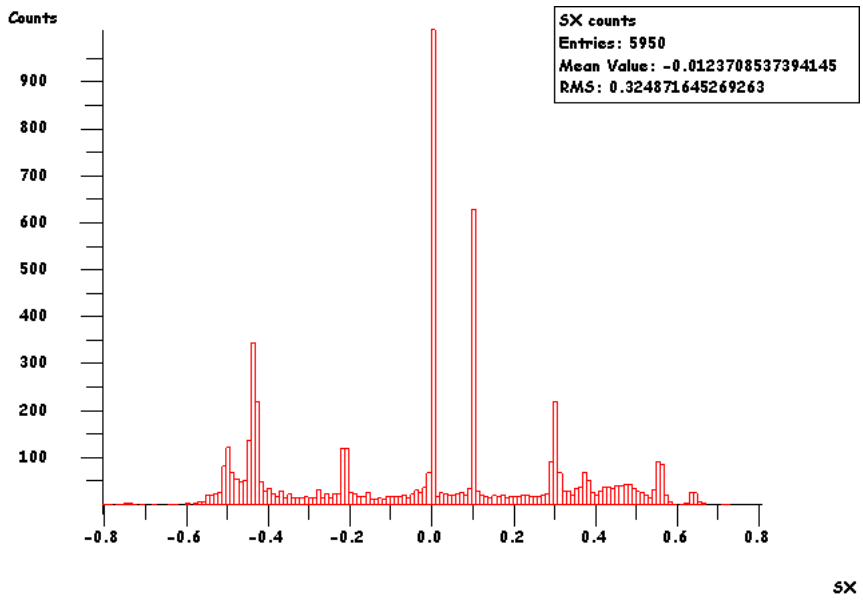

Figure 5.6: Results of a $1.5 \times 1.0\, cm^2$ area scanning.

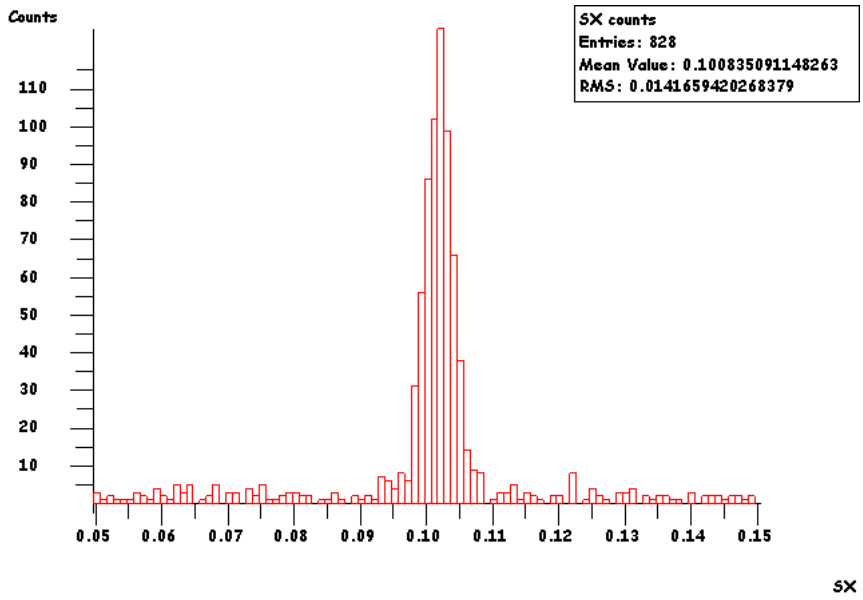

Figure 5.7: Results of a $1.5 \times 1.0\, cm^2$ area scanning around the slope 10mrad.

As it is seen the accuracy drops on higher angles, it is an expected result on scanning system because of detecting the particle with a high slope is more difficult for the system. Since the track is longer and the grains are more separated for the higher slope tracks the detection and image processing of such tracks is difficult for the system.

5.3.2 Precision Test

For the precision of the system we made twenty consecutive scanning of the same area and compared the results. Results are reported in the Figure 5.9. The results have taken with cut-off threshold as 300 and with the settings reported in the following figure:

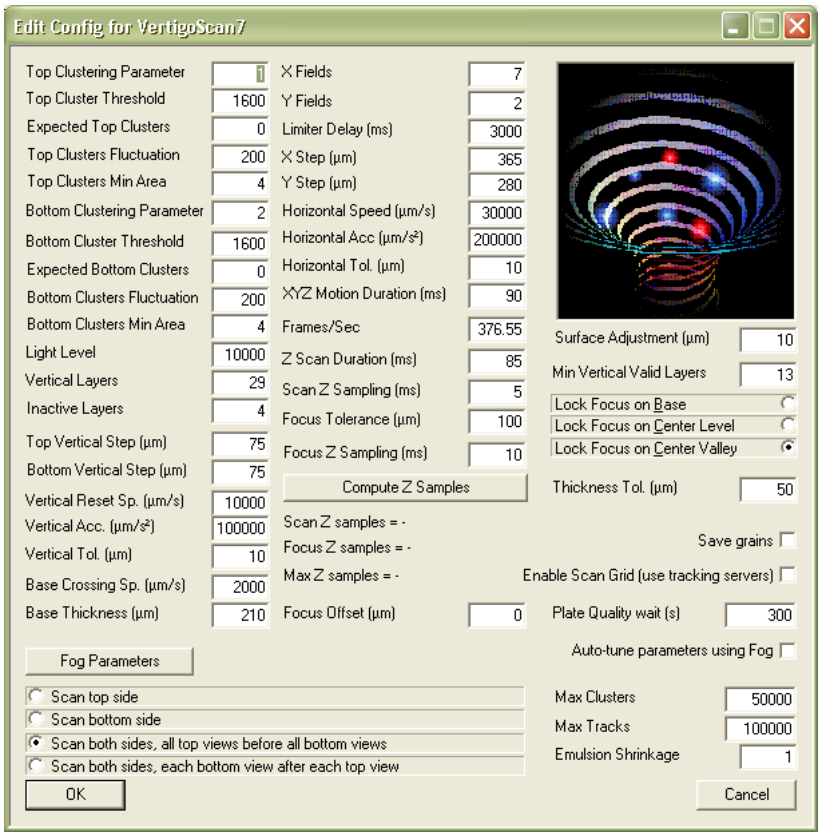

Figure 5.8: Precision Test made with these settings.

We have used the following quality cut: $sigma < 0.2 * N - 3.5$ where N is the number of grains of the track.

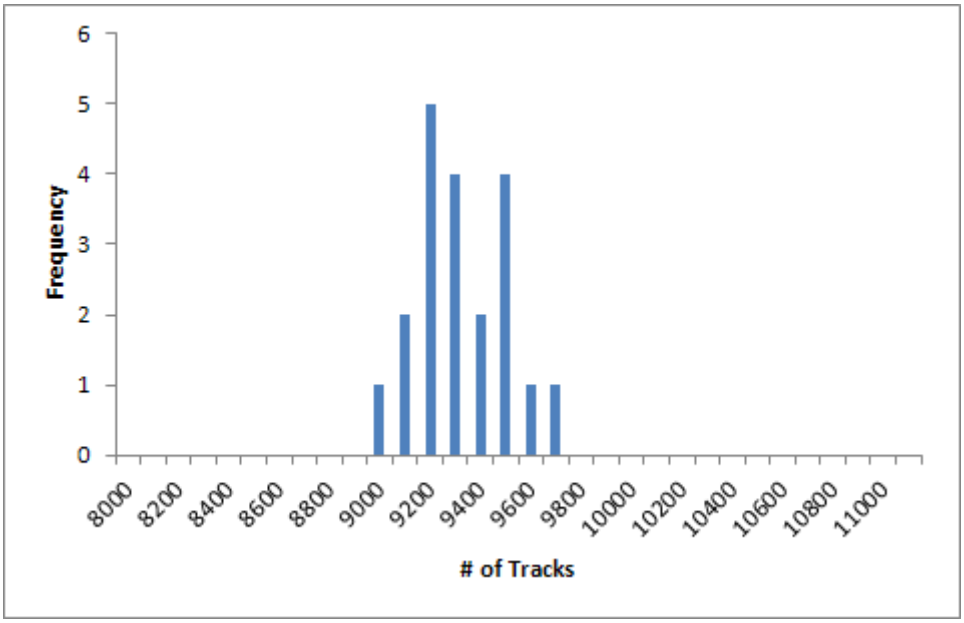

Figure 5.9: Repetition measurement for precision test

Mean of the 20 measurements after the quality cut: $\bar{x} = 9267$

The sigma calculation as follows:

$$\sigma = \sqrt{\frac{\sum (x - \bar{x})^2}{N - 1}} = 185.3639 \tag{5.3}$$

$$2\sigma = 370.7279 \tag{5.4}$$

From these calculations for a $1.5 \times 1.0 cm^2$ scanning area average number entries is 9267. Also calculations show that the number of entries in 68% of the measurements will have a maximum of 185 difference and in 95% of the calculations have a maximum of 271 difference.

If we taken account the possible outside effects during scanning period, $\sigma = 185$ is acceptable for 10000 events.

A possible outside effect is a small vibration of the system during a scanning period can affect

the results, another effect can be the focusing problems of the system on one or two zones which causes a data loss during scanning.

5.3.3 Tracking Efficency Test

Most of the particles in the OPERA experiment is passing through a number of emulsion plates before decaying. Locating the trails of a particle in each emulsion plate is crucial. The answer to the question: "How well the system tracks the trajectory of a charged particle in each emulsion plate?" is the *Tracking Efficiency*.

On a last step we made tests on the tracking efficiency and the results listed in the following table.

Table 5.2: Tracking Efficiency Test Results

Plates	Searched	Found	Efficiency
49-50-51	503	500	99.40%
50-51-52	561	560	99.82%

The tracking algorithm is expecting to find a number of tracks in all three consecutive plates after a special quality cut. Efficiency calculation is done by comparing the number of searched tracks and found tracks.

The same plates were scanned in Salerno in June and their efficiency result for three consecutive plates was 98% which is the nominal efficiency quoted in the OPERA proposal.

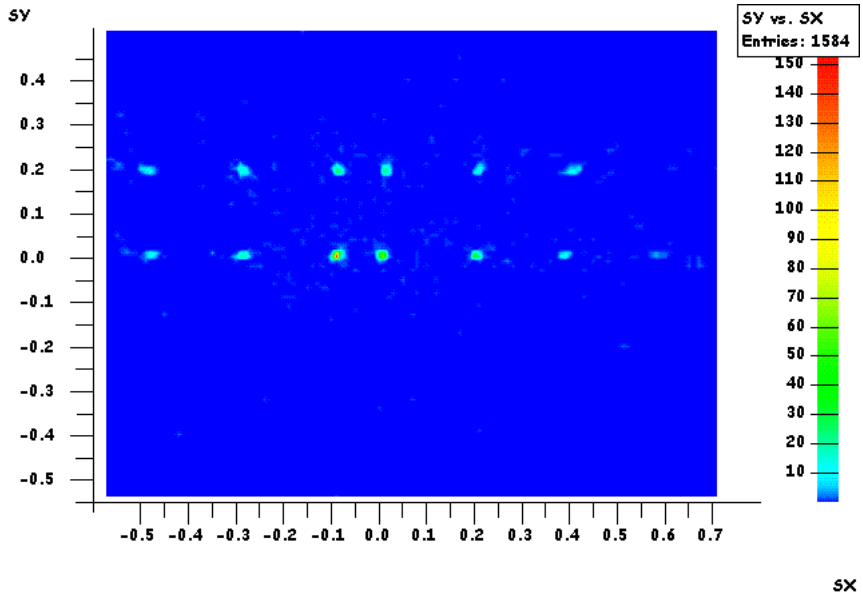

Figure 5.10: Beam angles for linked tracks.

Test results on tracking efficiency also satisfies the OPERA experiment criteria. The automatic scanning system in Ankara is ready for operating under OPERA experiment.

CHAPTER 6

Conclusion

The OPERA experiment aim is to verify the neutrino oscillation, directly measuring the appearance of ν_τ from an initially pure ν_μ beam produced at CERN. For this purpose the OPERA experiment is designed to be a long-baseline experiment operating 730km away. The OPERA detector located underground at LNGS and the detector structure designed to be a hybrid system consisting of emulsion targets and electronic detectors.

In OPERA experiment for a 5 years of data taking about 10 events are expected to be observed. In June, 2010, the OPERA Collaboration reported the first evidence for first ν_τ appearance in the CNGS beam. This first event is encouraging and observing few more τ lepton decays inevitably leads to an experimental proof of neutrino oscillations in an appearance mode.

It is important that to mention the importance of this automatic scanning system in conclusion. This laboratory has a unique feature in terms of experimental high energy physics laboratories. The emulsion scanning laboratory in METU is the first high energy laboratory in Turkey for data taking and data analysis at the same time.

The Emulsion Scanning Laboratory in Physics Department of METU is one of the scanning laboratories for the OPERA experiment. We successfully installed and completed the performance tests of the automatic scanning system. The performance of the scanning system is compatible with the other laboratories around Europe and Japan.

The system is ready for OPERA Experiment data taking and data analysis.

REFERENCES

[1] L. Bergstrom and A.Goobar, *Cosmology and Particle Astrophysics,* New York: Springer, 2006.

[2] Retrieved June 21, 2011, from http://hyperphysics.phy-astr.gsu.edu/hbase/ particles/cowan.html

[3] Retrieved June 11, 2011, from http://www.bnl.gov/bnlweb/history/nobel/nobel_88.asp

[4] DONuT Collaboration*, Final tau-neutrino results from the DONuT experiment,* PHYSICAL REVIEW D 78, 052002, 2008.

[5] S.L. Glashow, Nucl. Phys. 22 279, 1961.

[6] A. Salam, Phys. Rev. 127 331, 1962.

[7] S. Weinberg, Phys. Rev. Lett. 19 1264, 1967.

[8] P.W. Higgs, *Broken Symmetries and the Masses of Gauge Bosons,* Phys. Rev. Lett. 13, 508–509, 1964.

[9] D. H. Perkins, *Introduction to High Energy Physics, (4th edition),* United Kingdom: Cambridge University Press, 2000.

[10] B. Pontecorvo*, Neutrino Experiments and the Problem of Conservation of Leptonic Charge*, Sov. Phys. JETP 26: 984, 1968.

[11] Z. Maki, M. Nakagava and S. Sakata, *Neutrino Experiments and the Problem of Conservation of Leptonic Charge,* Sov.Phys.JETP 26:984-988, 1968.

[12] J.N. Bahcall, *Neutrino Astrophysics,* New York: Cambridge University Press, 1989.

[13] J. A. Thomas and P. L. Vahle, *Neutrino Oscillations, Present Status and Future Plans,* Singapore: World Scientific, 2007.

[14] Retrieved June 23, 2011, from http://neutrino.kek.jp/intro/k2k.html

[15] K2K Collaboration, *Measurement of Neutrino Oscillation by the K2K Experiment,* Phys. Rev. D 74, 072003 2006.

[16] Retrieved June 23, 2011, from http://www.sno.phy.queensu.ca/

[17] SNO Collaboration, *Independent Measurement of the Total Active* ^{8}*B Solar Neutrino Flux Using an Array of* ^{3}*He Proportional Counters at the Sudbury Neutrino Observatory,* PRL 101, 111301, 2008.

[18] Retrieved June 23, 2011, from http://www-numi.fnal.gov/

[19] MINOS Collaboration, *Measurement of the neutrino mass splitting and flavor mixing by MINOS,* FERMILAB-PUB-11-040-PPD & BNL-94498-2010-JA, 2011.

[20] T2K Collaboration*, Indication of Electron Neutrino Appearance from an Accelerator-produced Off-axis Muon Neutrino Beam,*Preprint submitted to PRL, 2011.

[21] J. J. Csathy, *Study of ν interactions and background estimation in the OPERA Emulsion Film Detector*, (Doctoral dissertation), University of Neuchatel, 2006.

[22] Retrieved February 01, 2011, from http://www.lngs.infn.it/lngs_infn/ index.htm?mainRecord=http://www.lngs.infn.it/lngs_infn/contents/lngs_en/public/visiting/

[23] A. Bettini, *Neutrino Physics at LNGS*, Presentation at DESY, 2003.

[24] C. Pistillo, *An automatic scanning system for nuclear emulsion analysis in the OPERA experiment*, (Doctoral dissertation), Universita degli Studi di Napoli, 2004.

[25] Retrieved February 01, 2011, from http://www.mi.infn.it/˜psala/Icarus/cngs.html

[26] Retrieved February 01, 2011, from http://operaweb.lngs.infn.it/spip.php?rubrique41

[27] Retrieved February 01, 2011, from http://proj-cngs.web.cern.ch/projcngs/Beam%20 Performance/BeamPerfor.htm

[28] B. Wonsak, *OPERA: A First ντ Appearance Candidate,* Presentation at DISCRETE2010

[29] C. Enrico, *The OPERA experiment: automated development of nuclear emulsions, installation and results of the Padova microscope*, (Doctoral dissertation), Universita degli studi di Padova, 2008.

[30] A. Cazes, S. Dusini and Y. Gornushkin, *Electronic Detectors*, Poster session presented at NU2010.

[31] N. Naganawa, *Emulsion Analysis in the OPERA Experiment,* Presentation at TAUP2009.

[32] S.Tufanlı, D^0 Background To Neutrino Oscillations In The OPERA Experiment, (Master's thesis), Middle East Technical University, 2009.

[33] P. Strolin, *OPERA Status Report,* Presentation, 2001.

[34] A. Russo, *Status of the OPERA experiment*, PoS(QFTHEP2010)081, 2010.

[35] OPERA Collaboration, *Observation of a first $\nu_\tau$candidate in the OPERA experiment in the CNGS beam,* Phys. Lett. B 691, 138-145, 2010.

[36] OPERA collaboration, M. Guler et al., *An appearance experiment to search for $\nu_\mu \rightarrow \nu_\tau$ oscillations in the CNGS beam: experimental proposal,* CERN-SPSC-2000-028, LNGS P25/2000

[37] OPERA collaboration, M. Guler et al., *Status Report on the OPERA experiment,* CERN/SPSC 2001-025, LNGS-EXP 30/2001 add. 1/01, 2001.

[38] Retrieved June 12, 2011, from http://images.iop.org/objects/ccr/ cern/50/6/1/CCnew1_06_10.jpg

[39] G. Sirri, *Automatic scanning of emulsion films for the OPERA experiment,* (Doctoral dissertation), Universita degli Studi di Bologna, 2003.

[40] Retrieved April 26, 2011, from http://www.micos-online.com/web2/en/1,4,420, ms8.html

[41] Retrieved April 26, 2011, from http://www.micos-online.com/web2/en/1,4,110, ls110.html

[42] Retrieved April 26, 2011, from http://en.wikipedia.org/wiki/Stepper_motor

[43] Retrieved April 26, 2011, from http://www.microscopyu.com/articles/ formulas/formulasworkingparfocal.html

[44] Retrieved April 26, 2011, from http://micro.magnet.fsu.edu/primer/anatomy/numaperture.html

[45] A. Andriani, G. De Lellis, I. Kreslo, C. Pistillo and C. Sirignano, *Report of test beam activity at CERN,* 2007.

[46] G. Sirri, *Mechanics and Optics Alignments,* Presentation.